Multi-step wind speed forecasting based on a hybrid forecasting architecture and an improved bat algorithm

Liye Xiao[a], Feng Qian[b], Wei Shao[a,*]

[a] *School of Physical Electronics, University of Electronic Science and Technology of China, Chengdu, China*[i]
[b] *Department of Electronic Engineering and Computer Science, Peking University, Beijing, China*

[ii]

Three potential referees suggested by authors:

Reviewer #1:
Name: Jinxing Che
Affiliation: College of Science, Nanchang Institute of Technology, Nanchang, Jiangxi, China
Email: jinxingche@163.com

Reviewer #2:
Name: Shanshan Qin
Affiliation: Department of Mathematics and Statistics, York University
Email: ssqin267@mathstat.yorku.ca

Reviewer #3:
Name: Hongya Xu
Affiliation: Arizona State University, Arizona, U.S.
Email: hong-ya.xu@asu.edu

i

ii

Abstract:

As one of the most promising sustainable energy sources, wind energy plays an important role in energy development because of its cleanliness without causing pollution. Generally, wind speed forecasting, which has an essential influence on wind power systems, is regarded as a challenging task. Analyses based on single-step wind speed forecasting have been widely used, but their results are insufficient in ensuring the reliability and controllability of wind power systems. In this paper, a new forecasting architecture based on decomposing algorithms and modified neural networks is successfully developed for multi-step wind speed forecasting. Four different hybrid models are contained in this architecture, and to further improve the forecasting performance, a modified bat algorithm (BA) with the conjugate gradient (CG) method is developed to optimize the initial weights between layers and thresholds of the hidden layer of neural networks. To investigate the forecasting abilities of the four models, the wind speed data collected from four different wind power stations in Penglai, China, were used as a case study. The numerical experiments showed that the hybrid model including the singular spectrum analysis and general regression neural network with CG-BA (SSA-CG-BA-GRNN) achieved the most accurate forecasting results in one-step to three-step wind speed forecasting.

Keywords: *hybrid forecasting architecture; improved bat algorithm; singular spectrum analysis, wind speed forecasting.*

Abbreviation

ANN	artificial neural network	GRNN	general regression neural network
ARIMA	autoregressive integrated moving average	MAE	mean absolute error
BA	bat algorithm	MAPE	mean absolute percentage error
CSA	cuckoo search algorithm	MSE	mean square error
CG	conjugate gradient	PSO	particle swarm optimization
EA	evolutionary algorithm	RBFNN	radical basis function neural network
EEMD	ensemble empirical mode decomposition	SDA	steepest descent algorithm
EMD	empirical mode decomposition	SSA	singular spectrum analysis
FEEMD	fast ensemble empirical mode decomposition	SVM	support vector machine
FVD	forecasting validity degree	WD	wavelet decomposition
GA	genetic algorithm	WPD	wavelet packet decomposition

Nomenclature

α	a random vector, with a value between 0 and 1.	M	total number of CG iterations
β	a random vector, with a value between 0 and 1	N	number of generations P
$\boldsymbol{d}_i^k$	the search direction of $\boldsymbol{x}_i$ at iteration k	O	output of RBFNN
d_i	Euclidian distance	r	pulse rate of a bat
ε	a random vector, with a value between 0 and 1	R	spread parameter
$\phi(d_i)$	outputs from the hidden layer of RBFNN	$r_n(t)$	nth residue
F_i	the fitness function of $\boldsymbol{x}_i$	σ	spread parameter
$-\nabla f\left(\boldsymbol{x}^{iter}\right)$	gradient of $\boldsymbol{x}^{iter}$	σ_j^i	marginal standard deviation
$\boldsymbol{g}_i^k$	gradient of $\boldsymbol{x}_i$ at iteration k	S_s	simple summation
h_j^i	correlation coefficient	S_w	weighted summation
I	input vector of RBFNN	t	current iteration number
$\mathbf{IMF}_j(t)$	intrinsic mode function	$\boldsymbol{v}_i^t$	the velocity of $\boldsymbol{x}_i$.at iteration t
$iter$	current iteration number	w	interconnection weight
$Iter_{\mathbf{max}}$	maximum number of iterations	w_i	weight of the hidden layer of RBFNN
K	shape matrix	X	input vector of GRNN
k_j^i	(i, j)th element of the shape matrix K	$\boldsymbol{x}_b$	the value of $\boldsymbol{x}$ with the best fitness value in the population
L	the loudness of a bat	$\boldsymbol{x}_t$	training data

m_i	center vector	$\boldsymbol{x}_i^t$	position of $\boldsymbol{x}_i$ at iteration t
m_i^j	jth element of center vector	$\boldsymbol{x}^{iter}$	positions of bats
λ_j^{iter}	step length	Y	output vector of GRNN
λ^k	step length of $\boldsymbol{x}_i$ at iteration k		

1. Introduction

As one of the most promising potential renewable energy sources [1], wind energy has attracted the focus of many researchers and scientists [2], and nearly every government across the world has introduced positive policies to support wind energy development [3, 4]. In 2015, the global total capacity of wind farms is approximately 432,419MW, with the 22% growth rate, as shown in **Fig. 1** [5]. With the increased proportion of wind energy in whole energy networks, accurate wind speed forecasting results are becoming increasingly crucial for managers to schedule the daily power distribution and decrease the reserve capacity. To protect wind power from the breakdown and make sure the success of wind power conversation, accurate forecasting results of wind speed are also required [6]. However, due to the non-stationary and nonlinear fluctuations, wind speed is regarded as one of the hardest weather parameters to predict [7, 8].

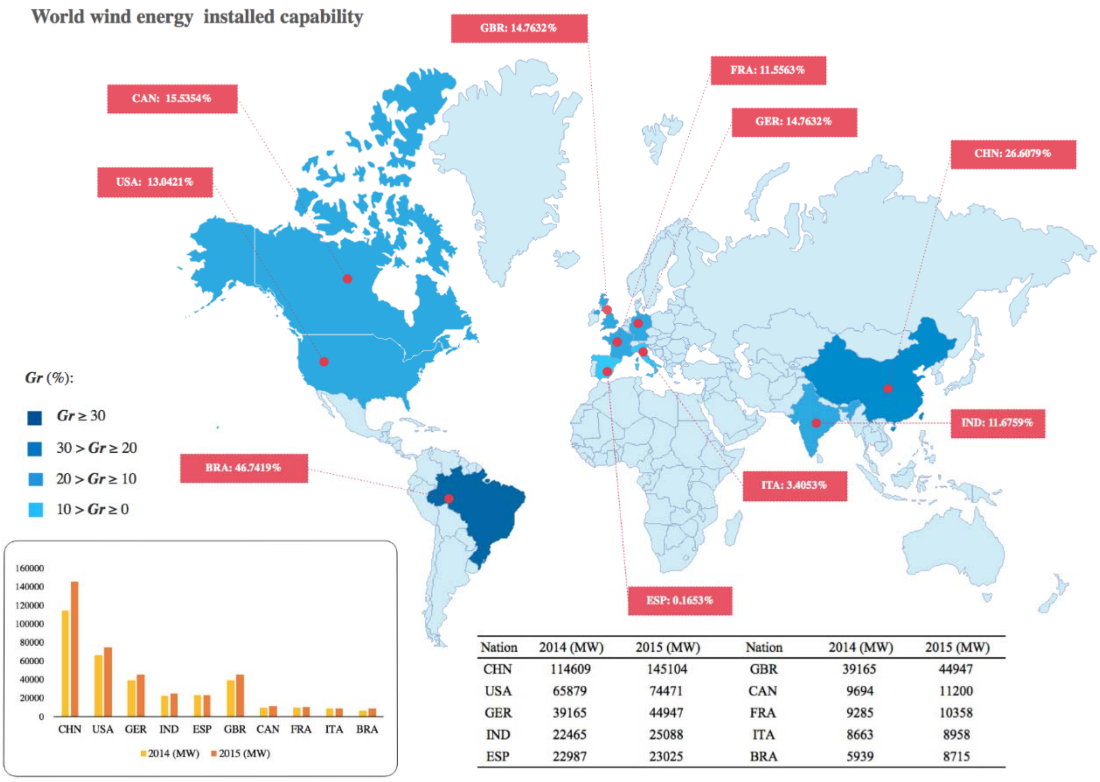

Nation	2014 (MW)	2015 (MW)	Nation	2014 (MW)	2015 (MW)
CHN	114609	145104	GBR	39165	44947
USA	65879	74471	CAN	9694	11200
GER	39165	44947	FRA	9285	10358
IND	22465	25088	ITA	8663	8958
ESP	22987	23025	BRA	5939	8715

Fig. 1. Top 10 countries of wind power newly increased installed capability in 2015.

In recent decades, many methods have been presented for wind speed forecasting, and these methods can be divided into four categories [9]: (a) physical models; (b) statistical models; (c) spatial correlation models; and (d) artificial intelligence models. Physical models which are based on physical parameters, such as topography, temperature and pressure, are usually applied in long term wind speed forecasting [10-12]. Statistical models are built based on the mature statistical equations to get the potential change rule from history data sampling [13-17]. Spatial correlation models mainly consider the spatial relationship of wind speed at different sites. In some situations, it can obtain higher precision [18, 19]. With the rapid development of artificial techniques, some artificial intelligence forecasting methods, including artificial neural networks (ANNs) [20-25], fuzzy logic methods [18, 26] and support vector machines (SVMs) [27], have been developed for wind speed forecasting.

Meanwhile, to decrease the negative influences that are intrinsic to individual models, many hybrid wind speed forecasting models have been proposed [28-36].

To achieve higher forecasting accuracy, some data-processing algorithms, such as wavelet decomposition (WD) [28], wavelet packet decomposition (WPD) [29], empirical mode decomposition (EMD) [30], the ensemble empirical mode decomposition (EEMD) algorithm [31] and the fast ensemble empirical mode decomposition (FEEMD) algorithm [32], have been employed in ANNs to build hybrid models. The data decomposition, which could reduce the non-stationary feature of the original data, promotes the forecasting performance indirectly.

Moreover, intelligent optimization algorithms including the genetic algorithm (GA) [33], particle swarm optimization (PSO) [34], the evolutionary algorithm (EA) [35], and the cuckoo search algorithm (CSA) [36], are utilized to determine the initial weights and thresholds of ANNs. In 2010, Yang proposed the bat algorithm (BA) [37], which is inspired by the echolocation characteristics of bats with varying pulse rates of emission and loudness. It has been applied to a wide range of optimization applications [38], including image processing [39], classifications [40], scheduling [41], the electricity market [42], energy systems [43] and various other problems. Experiments have shown its promising efficiency for global optimization.

Analyses based on single-step wind speed forecasting have been widely used, while their results are insufficient in ensuring the reliability and controllability of wind power systems. Thus, it is required to build a model to achieve accurate results for multi-step wind speed forecasting. Among various ANN models, the radical basis function neural network (RBFNN) and general regression neural network (GRNN) are good choices to achieve high convergence rates and accurate results. In this paper, a hybrid architecture, which contains four hybrid models, with two decomposing algorithms (i.e., FEEMD and singular spectrum analysis (SSA)) which are used to realize the non-stationary wind speed decomposition, and the modified RBFNN and GRNN is proposed for wind speed forecasting. In the modified RBFNN and GRNN, an improved BA, which is on the basis of conjugate gradient (CG) method to improve convergence performance over time and prevent individual bats from entrapment in local optima, is introduced to optimize the initial weights and thresholds of RBFNN and GRNN. The aim of this study is to investigate and enhance the forecasting performance of hybrid model based on signal processing algorithms, intelligent optimization algorithm and artificial neural networks for multi-step accurate wind speed forecasting. To investigate the forecasting abilities of the four models, the wind speed data collected from four different wind power stations in Penglai, China, were used as a case study. The main contributions in this paper are demonstrated as follows.

(1) ***The forecasting focus of the forecasting architecture is not only on the single-step forecasting but also on the multi-step forecasting.*** Although the wind speed single-step predictions have been studied widely, to protect the wind power, wind speed single-step forecasting results alone are insufficient, and wind speed multi-step forecasting results are definitely expected, thus the forecasting architecture is aim to enhance the forecasting accuracy of multi-step wind speed forecasting.

(2) ***To globally investigate the forecasting performance of different combination of decomposing algorithms and neural networks, a forecasting architecture contains four hybrid models is proposed.*** In the architecture, four different hybrid forecasting models based on the two most popular decomposing algorithms, an improved optimization algorithm and two neural networks, are investigated and compared (the performance of multi-step forecasting is given special attention in the investigation) with four different sites data for one-step to three-step forecasting to obtain the best one.

(3) ***The speed of local convergence and the accuracy of finding the optimal solution of BA are enhanced.*** To improve both the exploration and exploitation capacities and avoid the weakness of the local optima searching ability, the improved BA based on CG is proposed, and to evaluate the improved algorithm, four testing functions are used.

(4) ***The forecasting accuracy and stability of RBFNN and GRNN are enhanced.*** The improved BA, CG-BA, is employed to select the initial weights and thresholds for the RBFNN and GRNN. According to the experiment results, the forecasting performance of RBFNN and GRNN are directly enhanced with CG-BA.

(5) ***To validate the effectiveness of the proposed hybrid forecasting architecture, a number of comparable experiments are provided.*** Besides the hybrid FEEMD-CG-BA-RBFNN model, the hybrid FEEMD-CG-BA-GRNN model, the hybrid SSA-CG-BA-RBFNN model and the hybrid SSA-CG-BA-GRNN model, the single RBFNN model, the single GRNN model and the single ARIMA (autoregressive integrated moving average) model are also included in the performance comparison to obtain the best combination in the proposed architecture.

The remainder of the paper is organized as follows. Section 2 introduces the hybrid forecasting strategy proposed in this paper. Section 3 presents the wind speed decomposition contained in the hybrid forecasting strategy. Section 4 develops a new improved optimization algorithm. Section 5 proposes four hybrid models. The forecasting results of the proposed hybrid models and comparisons are discussed in Section 6. Finally, Section 7 concludes the paper.

2. Framework of the proposed hybrid architecture

The flowchart of the proposed hybrid architecture in this study is given in **Fig. 2**. In **Fig. 2**, the proposed study can be summarized briefly as follows:

- Decompose the original wind speed time series with the FEEMD algorithm and the SSA algorithm into several sub-layers.
- Build the modified neural networks, CG-BA-RBFNN and CG-BA-GRNN to predict each wind speed sub-layers for the one-step, two-step and three-step prediction.
- Summarize the one-step, two-step and three-step predicted results of each sub-layers from FEEMD and SSA to obtain the final results of CG-BA-RBFNN and CG-BA-GRNN.
- Compare the forecasting performance of each model and find the best one. The compared algorithms include four hybrid models, i.e. FEEMD-CG-BA-RBFNN,

FEEMD-CG-BA-GRNN, SSA-CG-BA-RBFNN and SSA-CG-BA-GRNN, in the proposed architecture, four comparison hybrid models, i.e. FEEMD-BA-RBFNN, FEEMD-BA-GRNN, SSA-BA-RBFNN and SSA-BA-GRNN and three single models, i.e. RBFNN, GRNN and ARIMA.

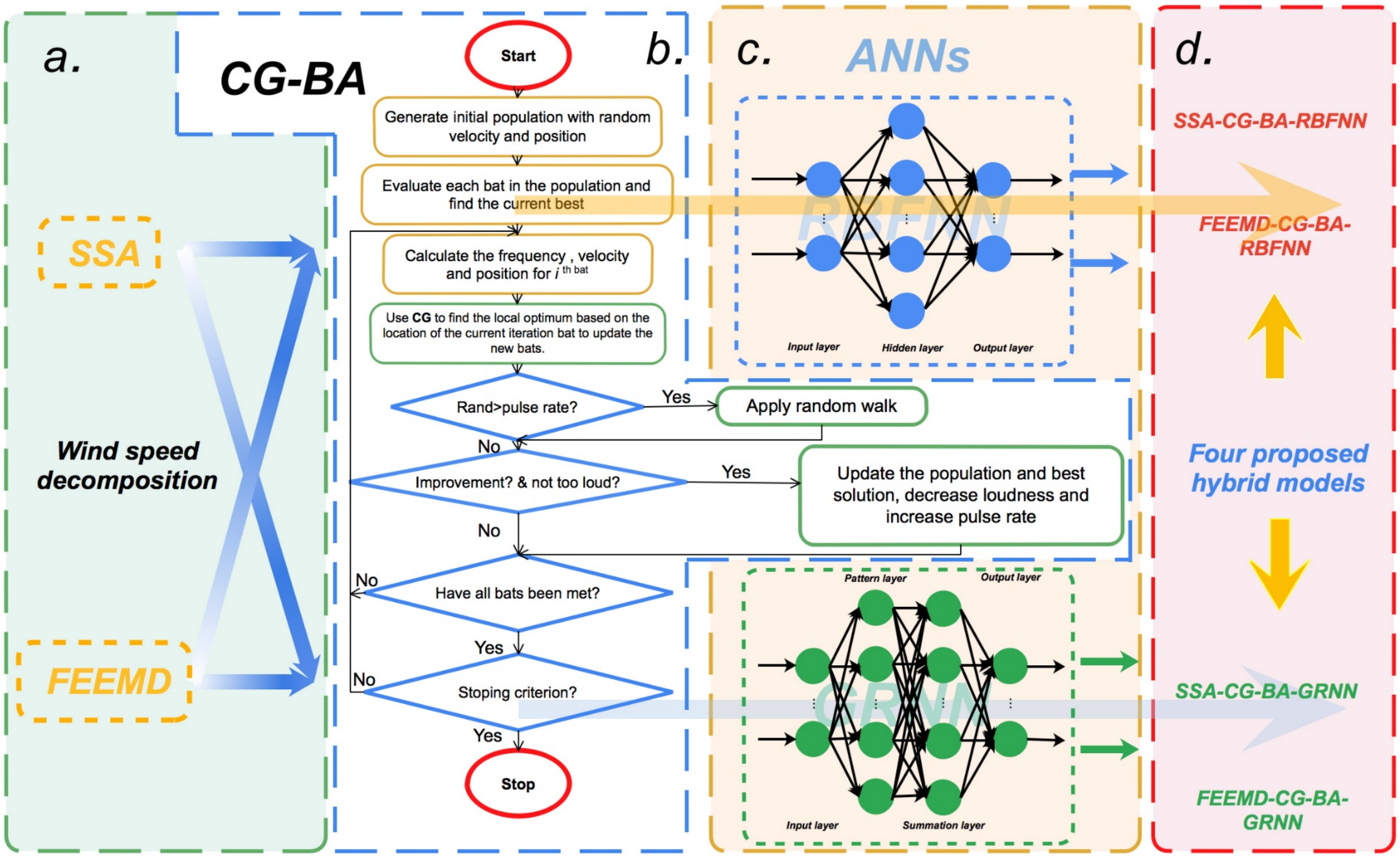

Fig. 2. Structure of hybrid forecasting strategy.

3. Wind speed decomposition

In this paper, two decomposing methods, the SSA algorithm and the FEEMD algorithm, are employed to process the original wind speed data. More information about SSA and FEEMD are shown in **Appendix A**.

4. CG-BA

In this part, CG-BA is proposed and four test functions are employed to evaluate this developed algorithm.

4.1 CG-BA

The bat algorithm is a novel optimization algorithm proposed by Yang [48, 49], which was inspired by the echolocation behavior of natural bats in determining their foods. BA not only offers powerful global exploration and exploitation abilities but also has the good ability to find the local optimum

However, conventional BA continues to suffer from slow convergence during the later period of optimization when it is applied to large-scale and complex problems. To speed up the convergence, a new improved BA based on the CG quasi-Newton method was developed in this work. CG is developed on the basis of the Newton algorithm and the steepest descent algorithm (SDA). Meanwhile, the shortcomings of these two algorithms, slow convergence of SDA and complex computation of Newton algorithm, are overcome with CG [50]. As shown in **Fig. 2 Part b**, it is used when BA updates solutions in an iteration to find a local optimal solution and thus enhance the local optimization ability and the speed of the local convergence of the whole algorithm.

Let $\boldsymbol{x}^{iter}$ be the positions of bats in BA, where *iter* represents the current iteration number. Generally, $\boldsymbol{x}^{iter}$ is input into the fitness function directly to evaluate the current best value. To improve the local search ability of BA, a CG circulation is added in BA. In this circulation, $\boldsymbol{x}^{iter}$ will be the initial value to continue searching with the gradient $-\nabla f\left(\boldsymbol{x}_j^{iter}\right)$ and step length λ_j^{iter}. This iterative loop could be presented as

$$\boldsymbol{x}_{j+1}^{iter} = \boldsymbol{x}_j^{iter} + \lambda_j^{iter}\boldsymbol{d}_j^{iter}, \left(j = 0, 1, \cdots, M-1\right) \tag{1}$$

where $\boldsymbol{d}_j^{iter} = -\nabla f\left(\boldsymbol{x}_j^{iter}\right)$, and M is the total number of CG iterations.

After processing the CG circulation, a new position of $\boldsymbol{x}_M^{iter}$ is obtained. $\boldsymbol{x}_M^{iter}$ is input into the fitness function to evaluate a value as the current best result. Then $\boldsymbol{x}_M^{iter}$ is updated to $\boldsymbol{x}_0^{iter+1}$ according to the BA rules [48, 49]. Meanwhile, to keep the results from trapping in local optimums, a lot of experiments have been done to select the total iteration number M. Finally we find that when M is set in the region from 4 to 6, the optimization performance is good. If M is less than 4, the rate of convergence may not be enhanced. And if M is greater than 6, the results are easily trapped in local optimums. The pseudo code for CG-BA is provided in **Algorithm 1**.

***Algorithm* 1: CG-BA**

***Output*:**

$\boldsymbol{x}_b$—the value of $\boldsymbol{x}$ with the best fitness value in the population

Parameters:

α—a random vector, with a value between 0 and 1.
ε—a random vector, with a value between 0 and 1.
β—a random vector, with a value between 0 and 1.
F_i—the fitness function of $\boldsymbol{x}_i$.
N—the number of generations P.
t—current iteration number.
$Iter_{\max}$—the maximum number of iterations.
M—the maximum number of iterations of conjugate gradient algorithm.
L—the loudness of a bat.
r—the pulse rate of a bat.
$\boldsymbol{v}_i^t$—the velocity of $\boldsymbol{x}_i$ at iteration t.
$\boldsymbol{x}_i^t$—the position of $\boldsymbol{x}_i$ at iteration t.
$\boldsymbol{g}_i^k$—the gradient of $\boldsymbol{x}_i$ at iteration k.
$\boldsymbol{d}_i^k$—the search direction of $\boldsymbol{x}_i$ at iteration k.
λ^k—the steplength of $\boldsymbol{x}_i$ at iteration k.

/*Initialize generation P ($\boldsymbol{x}_i$,i=1,2,…,N) in random positions.*/
/*Initialize t=0.*/
FOR EACH i=1:N **DO**
    Evaluate the corresponding fitness function F_i
END FOR
WHILE $t<Iter_{\max}$ **DO**
    FOR EACH i=1:N **DO**
        $F_i=F_{\min}+(F_{\max}-F_{\min})\alpha$
        $\boldsymbol{v}_i^t=\boldsymbol{v}_i^{t-1}+\left(\boldsymbol{x}_i^t-\boldsymbol{x}^*\right)F_i$
        $\boldsymbol{x}_i^t=\boldsymbol{x}_i^{t-1}+\boldsymbol{v}_i^t$
    END FOR
    /*Use conjugate gradient algorithm.*/
    FOR EACH k=1:M **DO**
        FOR EACH i=1:N **DO**
            $\boldsymbol{g}_i^k=\nabla F\left(\boldsymbol{x}_i^k\right)$
            $\varphi^{k-1}=\dfrac{\left\|\boldsymbol{g}^k\right\|^2}{\left\|\boldsymbol{g}^{k-1}\right\|^2}$
            $\boldsymbol{d}_i^k=-\boldsymbol{g}_i^k+\varphi^{k-1}\boldsymbol{d}_i^{k-1}$
            $\lambda^k=-\dfrac{\left(\boldsymbol{g}^k\right)^T\boldsymbol{d}^k}{\left(\boldsymbol{d}^k\right)^T A\boldsymbol{d}^k}$
            /*Where A is the symmetric positive definite matrix.*/
            $\boldsymbol{x}_i^{k+1}=\boldsymbol{x}_i^k+\lambda^k\boldsymbol{d}_i^k$
        END FOR
    END FOR
    /*Update the current best solution $\boldsymbol{x}$*.*/
    FOR EACH i=1:N **DO**
        Evaluate the corresponding fitness function F_i
    END FOR
    IF $F_{best}<F^*$ **THEN**
        FOR EACH i=1:N **DO**
            $\boldsymbol{x}_{new}=\boldsymbol{x}_{old}+\varepsilon L^t$
            IF $L^t>\beta$ **THEN**
                $L_i^{t+1}=\beta L_i^t$

```
                r_i^{t+1} = r_i^0 [1 − exp(−γt)]
            END IF
        END FOR
    END IF
    iter=iter+1
END WHILE
RETURN x_best
```

4.2 Test of CG-BA

To evaluate the proposed algorithm, CG-BA, four test functions are employed as shown in **Table 1**. Sphere function is unimodal, Rosenbrock's function is multimodal, Rastrigin's function is multimodal and Schaffer function is multimodal. The tests of BA and CG-BA on all test functions were performed on an Intel i7-4870 2.50 GHz machine with 16 GB RAM. The experimental parameters of BA and CG-BA are shown in **Table 2**.

As the test results shown in **Table 3**, two points can be concluded:

(a) The max value, min value and average value of iteration of CG-BA are less than the original BA for four test functions. This means the convergence ability of BA has been successfully improved with CG-BA.

(b) For the Rosenbrock's function, Rastrigin's function and Schaffer function, the convergence rates of BA didn't obtain 1. While for these three test functions, the convergence rates of CG-BA are obtained 1. Thus the optimization performance of the original BA has also enhanced with CG-BA.

Remark: Through the experimental results and above analysis, the optimization ability of the original BA has been successfully enhanced by the proposed CG-BA.

Table 1

Test functions

Function name	Modal characteristic	Test function	Variable domain	Global optimum
Sphere	Unimodal	$f(x)=\sum_{i=1}^{d} x_i^2$	$x_i \in [-5.12, 5.12]$	$f_{\min}(0,0,0\cdots 0)=0$
Rosenbrock	Multi-modal	$f(X)=\sum_{i=1}^{d-1}\left[100\left(x_i^2-x_{i+1}\right)^2+\left(x_i-1\right)^2\right]$	$x_i \in [-2.084, 2.084]$	$f_{\min}(1,1,1\cdots 1)=0$
Rastrigin	Multi-modal	$f(X)=\sum_{i=1}^{d}\left(x_i^2-10(2\pi x_i)+10\right)$	$x_i \in [-5.12, 5.12]$	$f_{\min}(0,0,0\cdots 0)=0$
Schaffer	Multi-modal	$f(X)=\dfrac{\sin^2\sqrt{\sum_{i=1}^{d} x_i^2}-0.5}{\left[1+0.001\left(\sum_{i=1}^{d} x_i^2\right)\right]^2}+0.5$	$x_i \in [-5.12, 5.12]$	$f_{\min}(0,0,0\cdots 0)=0$

Table 2

The experimental parameters of BA and CG-BA

Experimental parameters	BA	CG-BA
Maximum generation	10000	10000
Population size	100	100
Convergence tolerance	10^{-5}	10^{-5}
Maximum generation of CG	-	5

Table 3

Test results of BA and CG-BA

Test function	Dimension	Algorithm	Max value of iteration	Min value of iteration	Average value of iteration	Convergence rate
Sphere	10	BA	213	174	198	1
		CG-BA	3	1	1.4	1
	20	BA	343	151	182	1
		CG-BA	21	12	17.2	1
	50	BA	513	398	441	1
		CG-BA	112	84	98	1
Rosenbrock	2	BA	-	-	-	-
		CG-BA	165	79	103	1
Rastrigin	10	BA	421	315	369	1
		CG-BA	197	144	182	1
	20	BA	860	731	795	0.83
		CG-BA	528	378	469	1
	50	BA	-	-	-	-
		CG-BA	1342	873	1128	0.96
Schaffer	2	BA	1236	981	1035	0.81
		CG-BA	56	24	43	1

5. Optimization of RBFNN and GRNN

The proposed CG-BA is employed to optimize the initial weights and thresholds for the RBFNN and GRNN.

5.1 RBFNN optimized by CG-BA

This section contains the standard RBFNN and the improved RBFNN that is optimized by CG-BA.

5.1.1 Standard RBFNN

The structure of RBFNN is simple and includes an input layer, a hidden layer and an output layer, as shown in **Fig. 2 Part c**. The hidden layer is the key part of RBFNN, and its neurons represent RBFNN. More information about RBFNN is shown in **Appendix B**.

5.1.2 RBFNN optimized by CG-BA

The final results are dependent on the initial random weights and threshold values of an ANN, which will increase the unstable factor in forecasting. In this part of the paper, the CG-BA-RBFNN model is developed, and the proposed optimization algorithm CG-BA is used to optimize the initial weight and threshold of the RBFNN to improve the forecasting performance of RBFNN. The details of the CG-BA-RBFNN is presented as **Algorithm 2**.

***Algorithm* 2: CG-BA-RBFNN**

Input:

$x_t^{(0)} = \left(x^{(0)}(1), x^{(0)}(2), \ldots, x^{(0)}(q)\right)$–sequence of training wind speed data.

$x_v^{(0)} = \left(x^{(0)}(q+1), x^{(0)}(q+2), \ldots, x^{(0)}(q+d)\right)$–sequence of verification wind speed data

Output:

$\hat{y}_z^{(0)} = \left(\hat{y}^{(0)}(q+1), \hat{y}^{(0)}(q+2), \ldots, \hat{y}^{(0)}(q+d)\right)$—the forecasting electrical load data from RBFNN

Parameters:

α—a random vector, with a value between 0 and 1.

ε—a random vector, with a value between 0 and 1.

β—a random vector, with a value between 0 and 1.

F_i—the fitness function of x_i.

N—the number of generations P.

t—current iteration number.

$Iter_{\mathbf{max}}$—the maximum number of iterations.

M—the maximum number of iterations of conjugate gradient algorithm.
L—the loudness of a bat.
r—the pulse rate of a bat.
$\boldsymbol{x}_i$—generation *i* (the weight and threshold of the RBFNN)

Fitness function

$$F = \sum_{i=1}^{d} \left| \hat{x}_v^{(0)}(q+i) - \hat{y}_z^{(0)}(q+d) \right|$$

/*Initialize generation $\boldsymbol{X}$ ($\boldsymbol{x}_i$,i=1, 2,…, N, the weight and threshold of the RBFNN) in random positions.*/
/*Initialize t=0.*/
FOR EACH i=1:N **DO**
  Evaluate the corresponding fitness function F_i
END FOR
WHILE $t<Iter_{\max}$ **DO**
  FOR EACH i=1:N **DO**
    $F_i=F_{\min}+(F_{\max}-F_{\min})\alpha$
    $\boldsymbol{v}_i^t = \boldsymbol{v}_i^{t-1} + \left(\boldsymbol{x}_i^t - \boldsymbol{x}^*\right)F_i$
    $\boldsymbol{x}_i^t = \boldsymbol{x}_i^{t-1} + \boldsymbol{v}_i^t$
  END FOR
  /*Use conjugate gradient algorithm.*/
  FOR EACH k=1:M **DO**
    FOR EACH i=1:N **DO**
      $\boldsymbol{g}_i^k = \nabla F\left(\boldsymbol{x}_i^k\right)$
      $\varphi^{k-1} = \dfrac{\left\|\boldsymbol{g}^k\right\|^2}{\left\|\boldsymbol{g}^{k-1}\right\|^2}$
      $\boldsymbol{d}_i^k = -\boldsymbol{g}_i^k + \varphi^{k-1}\boldsymbol{d}_i^{k-1}$
      $\lambda^k = -\dfrac{\left(\boldsymbol{g}^k\right)^T \boldsymbol{d}^k}{\left(\boldsymbol{d}^k\right)^T A\boldsymbol{d}^k}$
      /*Where A is the symmetric positive definite matrix.*/
      $\boldsymbol{x}_i^{k+1} = \boldsymbol{x}_i^k + \lambda^k \boldsymbol{d}_i^k$
    END FOR
  END FOR
  /*Update the current best solution $\boldsymbol{x}^*$.*/
  FOR EACH i=1:N **DO**
    Evaluate the corresponding fitness function F_i
  END FOR
  IF $F_{best}< F^*$ **THEN**.
    FOR EACH i=1:N **DO**
      $\boldsymbol{x}_{new}=\boldsymbol{x}_{old}+\varepsilon L^t$

IF $L^t > \beta$ **THEN**

$L_i^{t+1} = \beta L_i^t$

$r_i^{t+1} = r_i^0\left[1-\exp(-\gamma t)\right]$

END IF

END FOR

END IF

$iter = iter + 1$

END WHILE

RETURN $\boldsymbol{x}_b$

Set the weight and threshold of the RBFNN according to $\boldsymbol{x}_b$.

Use $\boldsymbol{x}_t$ to train the RBFNN and update the weight and threshold of the RBFNN.

Input the historical data into RBFNN to obtain the forecasting value $\hat{y}$.

5.2 GRNN optimized by CG-BA

This section contains the standard GRNN and the improved GRNN that is optimized by CG-BA.

5.2.1 Standard GRNN

Specht [51] proposed a new type of neural network model named GRNN, which is based on the advantage of a standard statistical technology known as Kernel regression [52, 53]. Four layers, i.e., the input layer, pattern layer, summation layer, and output layer, compose a GRNN, as shown in **Fig. 2 Part c**. More information about GRNN is shown in **Appendix B**

5.2.2 GRNN optimized by CG-BA

This part proposed that the initial weight and threshold of the GRNN is optimized by the proposed optimization algorithm CG-BA to improve the forecasting performance. The details of the CG-BA-GRNN are presented as **Algorithm 3**.

***Algorithm* 3: CG-BA-GRNN**

Input:

$x_t^{(0)} = \left(x^{(0)}(1), x^{(0)}(2), \ldots, x^{(0)}(q)\right)$–sequence of training wind speed data.

$x_v^{(0)} = \left(x^{(0)}(q+1), x^{(0)}(q+2), \ldots, x^{(0)}(q+d)\right)$–sequence of verification wind speed data

Output:

$\hat{y}_z^{(0)} = \left(\hat{y}^{(0)}(q+1), \hat{y}^{(0)}(q+2), \ldots, \hat{y}^{(0)}(q+d)\right)$—the forecasting wind speed from GRNN

Parameters:

α—a random vector, with a value between 0 and 1.

ε—a random vector, with a value between 0 and 1.

β—a random vector, with a value between 0 and 1.

F_i—the fitness function of x_i.

N—the number of generations P.

t—current iteration number.

$Iter_{\mathbf{max}}$—the maximum number of iterations.

M—the maximum number of iterations of conjugate gradient algorithm.

L—the loudness of a bat.

r—the pulse rate of a bat.

$\boldsymbol{x}_i$—generation i (the weight and threshold of the GRNN)

Fitness function

$$F = \sum_{i=1}^{d} \left| \hat{x}_v^{(0)}(q+i) - \hat{y}_z^{(0)}(q+d) \right|$$

/*Initialize generation $\boldsymbol{X}(\boldsymbol{x}_i, i=1,2,\ldots,N,$ the weight and threshold of the GRNN) in random positions.*/

/*Initialize t=0.*/

FOR EACH i=1:N **DO**

  Evaluate the corresponding fitness function F_i

END FOR

WHILE $t<Iter_{\max}$ **DO**

  FOR EACH i=1:N **DO**

    $F_i=F_{\min}+(F_{\max}-F_{\min})\alpha$

    $\boldsymbol{v}_i^t = \boldsymbol{v}_i^{t-1} + \left(\boldsymbol{x}_i^t - \boldsymbol{x}^*\right) F_i$

    $\boldsymbol{x}_i^t = \boldsymbol{x}_i^{t-1} + \boldsymbol{v}_i^t$

  END FOR

  /*Use conjugate gradient algorithm.*/

  FOR EACH k=1:M **DO**

    FOR EACH i=1:N **DO**

      $\boldsymbol{g}_i^k = \nabla F\left(\boldsymbol{x}_i^k\right)$

      $\varphi^{k-1} = \dfrac{\left\|\boldsymbol{g}^k\right\|^2}{\left\|\boldsymbol{g}^{k-1}\right\|^2}$

      $\boldsymbol{d}_i^k = -\boldsymbol{g}_i^k + \varphi^{k-1}\boldsymbol{d}_i^{k-1}$

      $\lambda^k = -\dfrac{\left(\boldsymbol{g}^k\right)^T \boldsymbol{d}^k}{\left(\boldsymbol{d}^k\right)^T A\boldsymbol{d}^k}$

      /*Where A is the symmetric positive definite matrix.*/

      $\boldsymbol{x}_i^{k+1} = \boldsymbol{x}_i^k + \lambda^k \boldsymbol{d}_i^k$

    END FOR

  END FOR

/*Update the current best solution $\boldsymbol{x}^*$.*/

FOR EACH i=1:N **DO**

  Evaluate the corresponding fitness function F_i

END FOR

IF $F_{best} < F^*$ **THEN**.

  FOR EACH i=1:N **DO**

    $\boldsymbol{x}_{new} = \boldsymbol{x}_{old} + \varepsilon L^t$

    IF $L^t > \beta$ **THEN**

      $L_i^{t+1} = \beta L_i^t$

      $r_i^{t+1} = r_i^0 \left[1 - \exp(-\gamma t)\right]$

    END IF

  END FOR

END IF

$iter = iter + 1$

END WHILE

RETURN $\boldsymbol{x}_b$

Set the weight and threshold of the GRNN according to $\boldsymbol{x}_b$.

Use $\boldsymbol{x}_t$ to train the GRNN and update the weight and threshold of the GRNN.

Input the historical data into GRNN to obtain the forecasting value $\hat{y}$.

6. Forecasting experiment

In this part, the experiments were divided into three parts, ***Experiment I***, ***Experiment II*** and ***Experiment III***. In ***Experiment I***, the wind speed multi-step forecasting results and comparisons of the hybrid FEEMD-CG-BA-RBFNN model, the hybrid FEEMD-CG-BA-GRNN model, the hybrid SSA-CG-BA-RBFNN model and the hybrid SSA-CG-BA-GRNN model are given. In ***Experiment II***, the performance of the hybrid FEEMD-CG-BA-RBFNN model, the hybrid FEEMD-CG-BA-GRNN model, the hybrid SSA-CG-BA-RBFNN model and the hybrid SSA-CG-BA-GRNN model are compared with FEEMD-BA-RBFNN, FEEMD-BA-GRNN, SSA-BA-RBFNN, SSA-BA-GRNN, single RBFNN, single GRNN and ARIMA. In ***Experiment III***, the DM-test is used to evaluate the performance of each forecasting model. To confirm the universality of the proposed model, ***Experiment I***, ***Experiment II*** and ***Experiment III*** are validated at four different sites.

Four data sites in Penglai region have been selected as case our studies, with the latitude from 120°43’ N to 120°47’ N and longitude from37°50’ E to 37°37’ E. The data sites is in mountain and hilly area, the altitude ranges from 100 m to 240 m. The rated power of WTG (wind power generator) is 1500 KW, the height of measurement is 70 m. Penglai is entirely surrounded by Yantai, Shandong province with Fushan to the east, Longkou to the west, and Qixiato the south. The mean annual temperature, humidity and air pressure in this region are 11.9℃, 65% and 1012.7 hPa, respectively. Statistical parameters for the data used in this paper are shown in **Table 4**.

All algorithms are operated on the following platform: MATLAB R2012a on

Windows 8 with 2.50 GHz Intel Core i7 4870HQ 64-bit and 16 GB of RAM. The experimental parameters are shown in **Table 5**. Meanwhile, considering randomness factors and ensuring that the final results are reliable and independent of the initial weights, we carry out each experiment 50 times and then take the average value. The input layer of all the ANNs is constructed with four neurons. Hecht–Nelson method [54] is employed to determine the node number of the hidden layer. When the node number of the input layer is n, the node number of the hidden layer is $2n + 1$.

Table 4

Statistical parameters for the data used in this paper

Region	Mean value (m/s)	Std. dev. (m/s)	Maximum value (m/s)	Minimum value (m/s)	Median value (m/s)
Site 1	6.5564	2.4147	14.3000	1.4000	6.3000
Site 2	5.8237	2.1162	15.7000	0.9000	5.6000
Site 3	7.8363	3.4319	18.3000	1.0000	7.1000
Site 4	6.4602	2.5402	17.2000	0.8000	6.3000

Table 5

Experimental parameter setting

Model	Experimental parameters	Default value
GRNN	Neuron number of the input layer	4
	Neuron number of the hidden layer	9
	Neuron number of the output layer	1
	Radial basis function expansion	0.1 to 2.0
	Maximum number of training	1000
	Training requirement precision	0.00002
RBFNN	Neuron number of the input layer	4
	Neuron number of the hidden layer	9
	Neuron number of the output layer	1
	Sample	400
	Maximum number of training	1000
	Training requirement precision	0.00002

6.1 Accuracy estimating indexes

To learn the global traits of the models, three metric parameters are taken: the MAE (mean absolute error), the MAPE (mean absolute percentage error) and the MSE (mean square error). MAE is the average absolute forecast error of n times forecast results. Because the prediction error may be positive and negative, the absolute error cannot reflect the level of error; this problem can be avoided by using the MAE. MSE is the average of the prediction error squares, which can evaluate the change of the prediction model; the smaller is the MSE value, the better is the prediction model. MAPE is a measure of the accuracy of the prediction method for use in the performance evaluation and comparison in statistics. The detailed equations of these three error indexes are given in **Appendix C**.

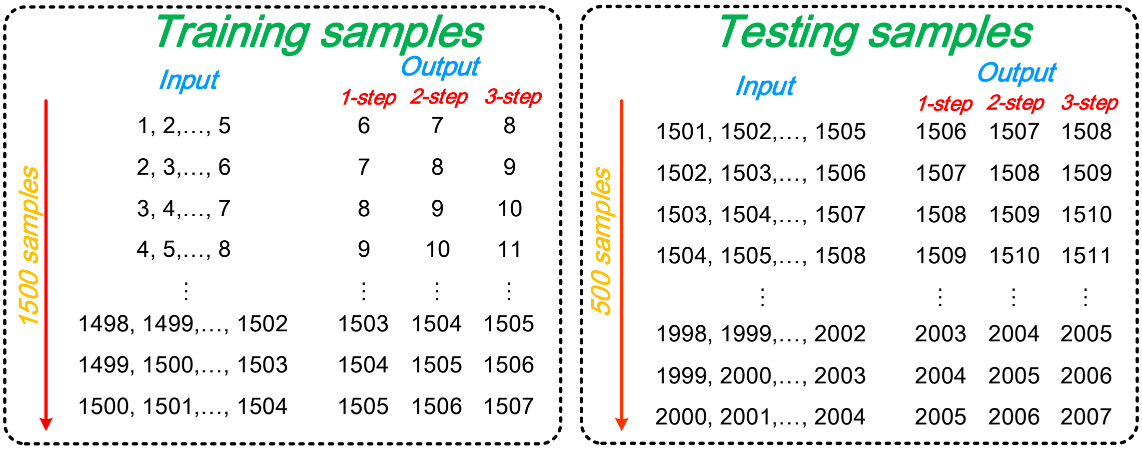

Fig. 3 Input and output data selection.

6.2 Experiment I

The data from four wind power stations in Penglai, China are used as test data in this experiment, we chose 1500 history data for training and 500 data for testing as shown in **Fig. 3**. The multi-step forecasting results of SSA-CG-BA-RBFNN, SSA-CG-BA-GRNN, FEEMD-CG-BA-RBFNN and FEEMD-CG-BA-GRNN are shown in **Table 6** and **Fig. 4**. The detailed multi-step promoting percentages of the hybrid models of the four sites are shown in **Table 7** and **Fig. 5**.

Table 6 and **Fig. 4** indicate the following:

(a) For Site 1, when the forecasting is 1-step, SSA-CG-BA-GRNN has the highest accuracy forecasting results with a 1.2720% MAPE value. The second-highest to fourth-highest accurate models are FEEMD-CG-BA-GRNN, SSA-CG-BA-RBFNN and FEEMD-CG-BA-RBFNN with MAPE values of 1.3752%, 1.6510% and 1.9053%, respectively. When the forecasting is 2-step, SSA-CG-BA-GRNN has the most accurate forecasting results with a MAPE value of 2.9528%. According to the MAPE value, FEEMD-CG-BA-GRNN is the second most accurate model, SSA-CG-BA-RBFNN is the third most accurate model and FEEMD-CG-BA-RBFNN is the fourth most accurate model with MAPE values of 3.0261%, 3.2489% and 3.4029%, respectively. When the forecasting is 3-step, SSA-CG-BA-GRNN is still the most accurate forecasting model among the proposed four hybrid models.

(b) For Site 2, SSA-CG-BA-GRNN has the most accurate forecasting results among the 1.2720%, 2.7491% and 3.8576%, respectively. When the forecasting is 2-step, FEEMD-CG-BA-RBFNN is more accurate than SSA-CG-BA-RBFNN. In the three-step forecasting, the precision of the hybrid models is ranked from high to low as SSA-CG-BA-GRNN, FEEMD-CG-BA-GRNN, SSA-CG-BA-RBFNN and FEEMD-CG-BA-RBFNN.

(c) SSA-CG-BA-GRNN is the most accurate model for one-step to three-step forecasting among the four hybrid models in Site 3. The CG-BA-RBFNN with the SSA decomposition algorithm is more precise than CG-BA-RBFNN with the FEEMD algorithm.

(d) SSA-CG-BA-GRNN is still the most accurate forecasting model from one-step forecasting to three-step forecasting among all of the proposed models for the data from Site 4. However, for this site, the two-step forecasting results of SSA-CG-BA-RBFNN are more accurate than FEEMD-CG-BA-GRNN.

Table 6

Forecasting performance of four proposed hybrid models

		SSA-CG-BA-RBFNN			SSA-CG-BA-GRNN			FEEMD-CG-BA-RBFNN			FEEMD-CG-BA-GRNN		
		1-step	**2-step**	**3-step**	**1-step**	**2-step**	**3-step**	**1-step**	**2-step**	**3-step**	**1-step**	**2-step**	**3-step**
	MAE	0.0906	0.1783	0.2799	0.0698	0.1621	0.2334	0.1047	0.1869	0.2963	0.0755	0.1661	0.2581
Site 1	MSE	0.0091	0.0353	0.0871	0.0054	0.0291	0.0605	0.0122	0.0389	0.0977	0.0063	0.0306	0.0740
	MAPE(%)	1.6510	3.2489	5.1002	1.2720	2.9528	4.2507	1.9053	3.4029	5.3953	1.3752	3.0261	4.7022
	MAE	0.1011	0.2155	0.3121	0.0773	0.1767	0.2483	0.0948	0.2024	0.3379	0.0862	0.1881	0.2861
Site 2	MSE	0.0122	0.0555	0.1163	0.0071	0.0373	0.0738	0.0107	0.0489	0.1364	0.0089	0.0422	0.0977
	MAPE(%)	1.5737	3.3484	4.8506	1.2016	2.7491	3.8576	1.4738	3.1483	5.2544	1.3405	2.9228	4.4539
	MAE	0.0938	0.2195	0.3241	0.0851	0.1755	0.2587	0.0955	0.2127	0.3472	0.0903	0.2088	0.3121
Site 3	MSE	0.0105	0.0574	0.1252	0.0086	0.0367	0.0795	0.0108	0.0538	0.1435	0.0097	0.0519	0.1159
	MAPE(%)	1.3249	3.0974	4.5735	1.2031	2.4749	3.6545	1.3478	3.0035	4.8984	1.2746	2.9477	4.4049
	MAE	0.1001	0.2193	0.3633	0.0919	0.2031	0.2846	0.1042	0.2251	0.3645	0.0975	0.2215	0.2903
Site 4	MSE	0.0114	0.0548	0.1502	0.0096	0.0469	0.0922	0.0123	0.0577	0.1513	0.0108	0.0559	0.0959
	MAPE(%)	1.3448	2.9471	4.8832	1.2347	2.7263	3.8254	1.4008	3.0241	4.8963	1.3099	2.9763	4.3003

Fig. 4. Forecasting results of four proposed hybrid models.

Table 7 and **Fig. 5** shows the following:

(a) In the one-step predictions, the ξ_{MAPE}(%) value indicates that, from four sites, the MAPE value of SSA-CG-BA-RBFNN, FEEMD-CG-BA-GRNN and FEEMD-CG-BA-RBFNN are decreased with SSA-CG-BA-GRNN with -22.956, -23.645, -9.193 and -8.187; 8.113, 11.560, 5.943 and 6.091; -16.705, -14.819, -3.797 and -2.595, respectively.

(b) In the two-step and three-step predictions, SSA-CG-BA-GRNN also decreases the MAPE value based on SSA-CG-BA-RBFNN, FEEMD-CG-BA-GRNN and FEEMD- CG-BA-RBFNN.

(c) In the one-step predictions, the ξ_{MAPE}(%) value illustrates that from four sites, FEEMD-CG-BA-GRNN decreases 27.822%, 9.045%, 5.431% and 6.489% MAPE values based on FEEMD-CG-BA-RBFNN. In the two-step predictions, FEEMD-CG-BA-GRNN decreases 11.073%, 7.163%, 1.858% and 1.581% MAPE values based on FEEMD-CG-BA-RBFNN. 12.846%, 15.235%, 10.075% and 12.172% MAPE values are decreased with FEEMD-CG-BA-GRNN based on FEEMD-CG-BA-RBFNN in the three-step predictions, respectively.

Remark

By comparing the four proposed hybrid models, the SSA-CG-BA-GRNN hybrid model has the most accurate forecasting results. Comparisons of FEEMD-CG-BA-GRNN with FEEMD-CG-BA-RBFNN and SSA-CG-BA-GRNN with SSA-CG-BA-RBFNN could conclude that the forecasting ability of GRNN is stronger than that of RBFNN. Comparisons of SSA-CG-BA-GRNN with FEEMD-CG-BA-GRNN and SSA-CG-BA-RBFNN with FEEMD-CG-BA-GRNN could reveal that the hybrid models combined with SSA are more accurate than the hybrid models combined with FEEMD.

Table 7

Improvement percentages of four proposed hybrid models

		SSA-CG-BA-RBFNN *vs.* SSA-CG-BA-GRNN			SSA-CG-BA-RBFNN *vs.* FEEMD-CG-BA-RBFNN			SSA-CG-BA-RBFNN *vs.* FEEMD-CG-BA-GRNN		
		1-step	**2-step**	**3-step**	**1-step**	**2-step**	**3-step**	**1-step**	**2-step**	**3-step**
	ξ_{MAE}(%)	-22.958	-9.086	-16.613	15.563	4.823	5.859	-16.667	-6.842	-7.788
Site 1	ξ_{MSE}(%)	-40.659	-17.564	-30.540	34.066	10.198	12.170	-30.769	-13.314	-15.040
	ξ_{MAPE}(%)	-22.956	-9.114	-16.656	15.403	4.740	5.786	-16.705	-6.858	-7.804
	ξ_{MAE}(%)	-23.541	-18.005	-20.442	-6.231	-6.079	8.267	-14.738	-12.715	-8.331
Site 2	ξ_{MSE}(%)	-41.803	-32.793	-36.543	-12.295	-11.892	17.283	-27.049	-23.964	-15.993
	ξ_{MAPE}(%)	-23.645	-17.898	-20.472	-6.348	-5.976	8.325	-14.819	-12.711	-8.178
	ξ_{MAE}(%)	-9.275	-20.046	-20.179	1.812	-3.098	7.127	-3.731	-4.875	-3.703
Site 3	ξ_{MSE}(%)	-18.095	-36.063	-36.502	2.857	-6.272	14.617	-7.619	-9.582	-7.428
	ξ_{MAPE}(%)	-9.193	-20.098	-20.094	1.728	-3.032	7.104	-3.797	-4.833	-3.686
	ξ_{MAE}(%)	-8.192	-7.387	-21.663	4.096	2.645	0.330	-2.597	1.003	-20.094
Site 4	ξ_{MSE}(%)	-15.789	-14.416	-38.615	7.895	5.292	0.732	-5.263	2.007	-36.152
	ξ_{MAPE}(%)	-8.187	-7.492	-21.662	4.164	2.613	0.268	-2.595	0.991	-11.937

		SSA-CG-BA-GRNN *vs.* FEEMD-CG-BA-RBFNN			SSA-CG-BA-GRNN *vs.* FEEMD-CG-BA-GRNN			FEEMD-CG-BA-RBFNN *vs.* FEEMD-CG-BA-GRNN		
		1-step	**2-step**	**3-step**	**1-step**	**2-step**	**3-step**	**1-step**	**2-step**	**3-step**
	ξ_{MAE}(%)	50.000	15.299	26.949	8.166	2.468	10.583	-27.889	-11.129	-12.892
Site 1	ξ_{MSE}(%)	125.926	33.677	61.488	16.667	5.155	22.314	-48.361	-21.337	-24.258
	ξ_{MAPE}(%)	49.788	15.243	26.927	8.113	2.482	10.622	-27.822	-11.073	-12.846
	ξ_{MAE}(%)	22.639	14.544	36.085	11.514	6.452	15.224	-9.072	-7.065	-15.330
Site 2	ξ_{MSE}(%)	50.704	31.099	84.824	25.352	13.137	32.385	-16.822	-13.701	-28.372
	ξ_{MAPE}(%)	22.653	14.521	36.209	11.560	6.318	15.458	-9.045	-7.163	-15.235
	ξ_{MAE}(%)	12.221	21.197	34.210	6.110	18.974	20.642	-5.445	-1.834	-10.109
Site 3	ξ_{MSE}(%)	25.581	46.594	80.503	12.791	41.417	45.786	-10.185	-3.532	-19.233
	ξ_{MAPE}(%)	12.027	21.358	34.037	5.943	19.104	20.534	-5.431	-1.858	-10.075
	ξ_{MAE}(%)	13.384	10.832	28.074	6.094	9.060	2.003	-6.430	-1.599	-20.357
Site 4	ξ_{MSE}(%)	28.125	23.028	64.100	12.500	19.190	4.013	-12.195	-3.120	-36.616
	ξ_{MAPE}(%)	13.453	10.923	27.994	6.091	9.170	12.414	-6.489	-1.581	-12.172

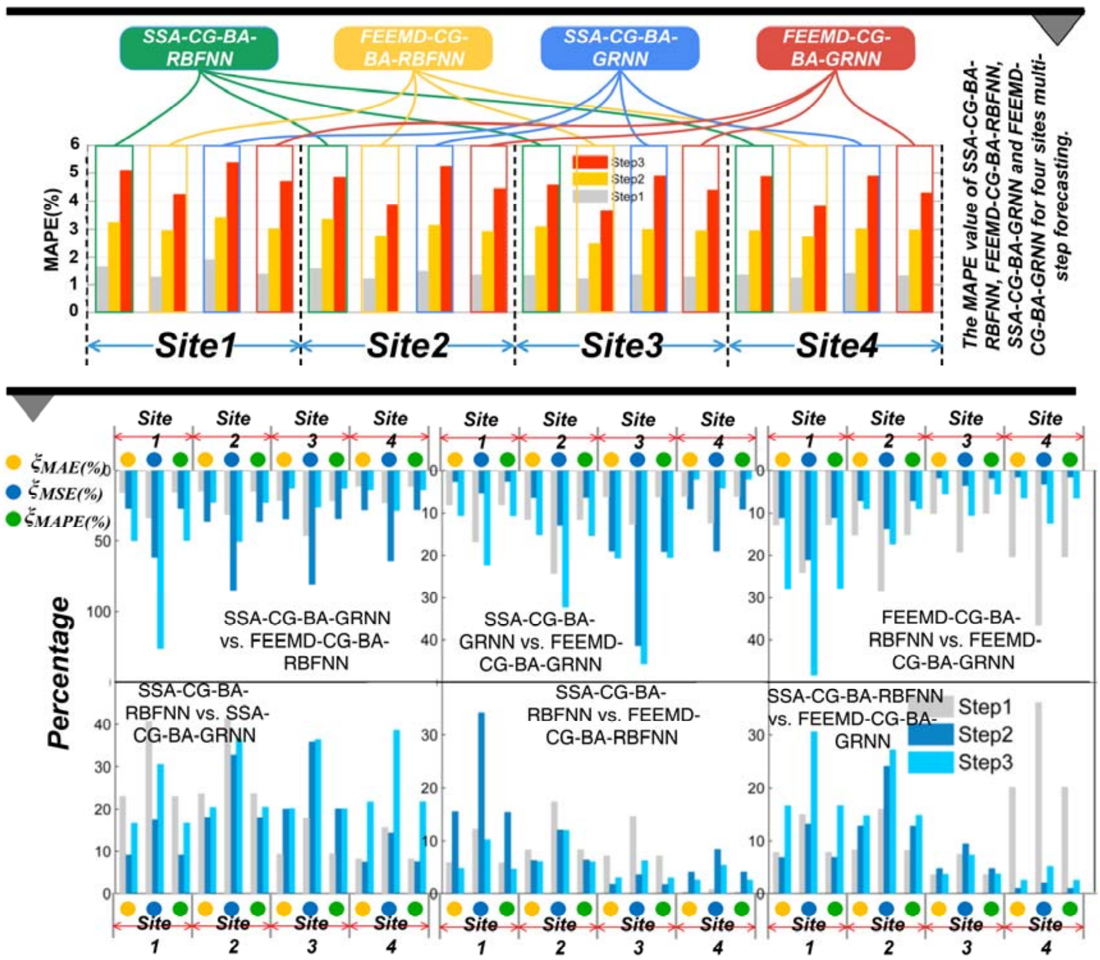

Fig. 5. Promoting percentages of four hybrid models.

6.3 Experiment II

This experiment is divided into two parts. The first part illustrates the multi-step forecasting results of SSA-BA-RBFNN, SSA-BA-GRNN, FEEMD-BA-RBFNN and FEEMD-BA-GRNN (as shown in **Table 8** and **Fig. 6**) and the detailed multi-step promoting percentages, using the data from four sites, to evaluate the efficiency of the developed optimization algorithm CG-BA (as shown in **Table 9** and **Fig. 6**). In the second part, five single models, ELM, SVM, RBFNN, GRNN and ARIMA, are employed in multi-step prediction (as shown in **Tables 10-11**). The detailed multi-step promoting percentages of SSA-CG-BA-RBFNN, SSA-CG-BA-GRNN, FEEMD-CG-BA-RBFNN and FEEMD-CG-BA-GRNN by RBFNN, GRNN and ARIMA of four sites are shown in **Tables 12–13**.

Table 8 shows the following:

(a) SSA-BA-GRNN achieves the highest accuracy in one-step prediction to three-step prediction based on the data from four sites.

(b) FEEMD-BA-GRNN is ranked as the second most accurate model among the four models listed in **Table 5**, except for two-step prediction at Site 4.

(c) The forecasting accuracy of BA-RBFNN with the decomposition algorithms SSA and FEEMD is lower than that of BA-GRNN with the decomposition algorithms SSA and FEEMD, mostly.

Table 9 illustrates the following:

(a) In the one-step to three-step predictions, SSA-BA-RBFNN decreases the MAPE values from four sites based on SSA-CG-BA-RBFNN are 6.6862%, 3.9412% and 3.1007%;11.081%, 8.1497% and 6.4277%; 19.169%, 8.6555% and 10.541% and 21.384%, 9.3646% and 5.4413%, respectively.

(b) For the data from four sites, SSA-BA-GRNN decreases the MAPE values in the one-step to three-step predictions on the basis of SSA-CG-BA-GRNN are 15.431%, 2.7884% and 10.739%;28.472%, 7.0181% and 5.9328%; 20.456%, 20.182% and 10.733% and 24.763%, 14.197% and 9.5735%, respectively.

(c) The $\xi_{MAPE}(\%)$ values presents that from four sites in the one-step to three-step predictions, the MAPE values are decreased with 16.257%, 9.5431% and 3.3758%; 16.228%, 11.5025% and 5.8722%; 24.917%, 12.969% and 7.3186% and 24.724%, 12.641% and 7.3531% with FEEMD-CG-BA-RBFNN based on FEEMD-BA-RBFNN, respectively.

(d) In the one-step to three-step predictions, the MAPE values from four sites of by FEEMD-BA-GRNN are decreased 21.649%, 10.131% and 12.037%; 17.796%, 15.143% and 15.838%; 25.182%, 14.333% and 7.0716% and 25.229%, 9.4551% and 13.659% with FEEMD-CG-BA-GRNN, respectively.

Remark

By comparing SSA-CG-BA-RBFNN, SSA-CG-BA-GRNN, FEEMD-CG-BA-RBFNN and FEEMD-CG-BA-GRNN with SSA-BA-RBFNN, SSA-BA-GRNN, FEEMD-BA-RBFNN and FEEMD-BA-GRNN, the performance of the proposed optimization algorithm CG-BA is better than that of the original BA.

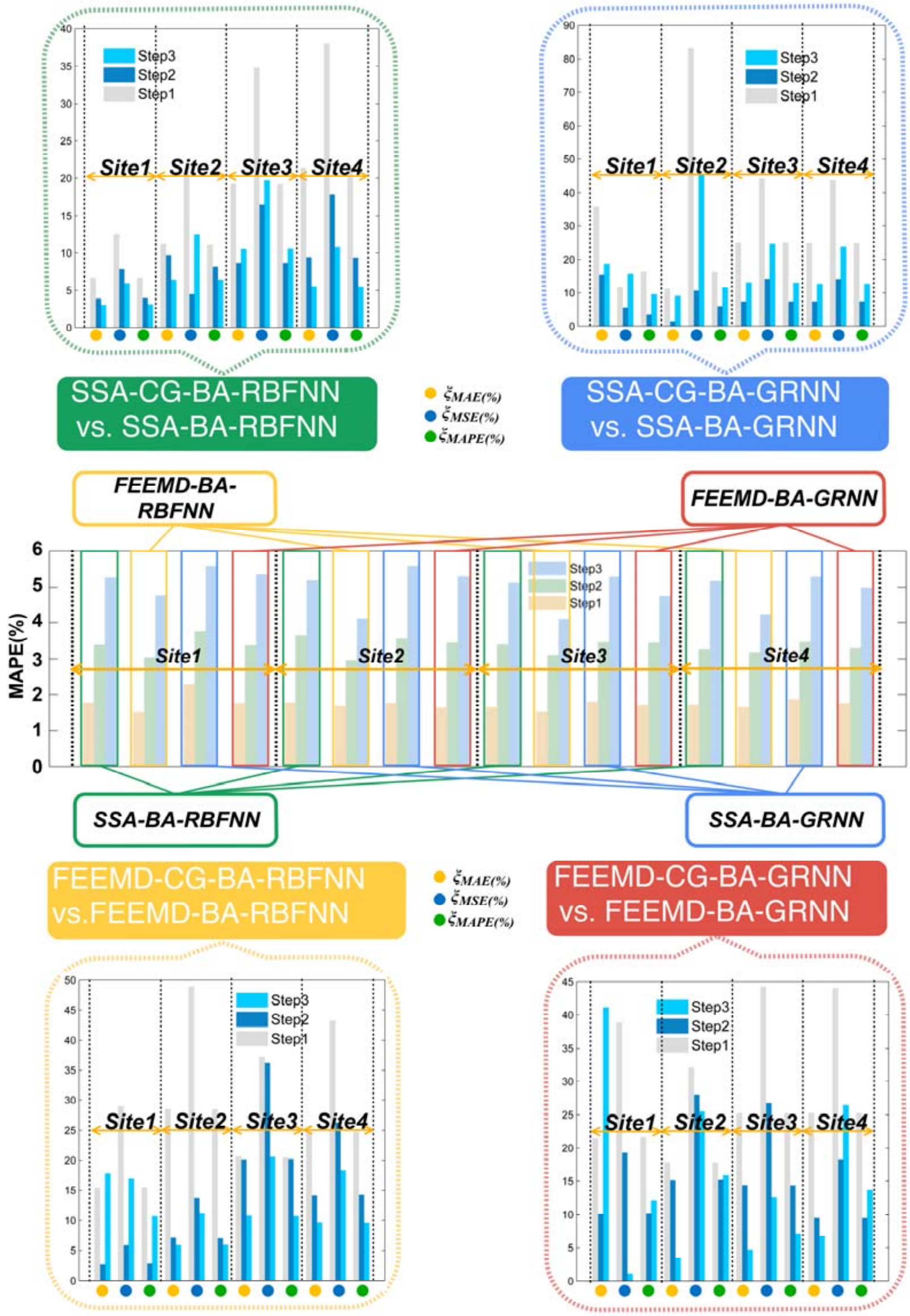

Fig. 6. Forecasting results and promoting percentages of SSA-BA-RBFNN, FEEMD-BA-RBFNN, SSA-BA-GRNN and FEEMD-BA-GRNN.

Table 8

Forecasting performance of SSA-BA-RBFNN, SSA-BA-GRNN, FEEMD-BA-RBFNN and FEEMD-BA-GRNN

		SSA-BA-RBFNN			SSA-BA-GRNN			FEEMD-BA-RBFNN			FEEMD-BA-GRNN		
		1-step	**2-step**	**3-step**	**1-step**	**2-step**	**3-step**	**1-step**	**2-step**	**3-step**	**1-step**	**2-step**	**3-step**
	MAE	0.0971	0.1855	0.2886	0.0825	0.1665	0.2838	0.1628	0.2298	0.3498	0.0962	0.1846	0.4383
Site 1	MSE	0.0104	0.0383	0.0926	0.0076	0.0309	0.0728	0.0138	0.0461	0.1034	0.0103	0.0379	0.0732
	MAPE(%)	1.7693	3.3822	5.2634	1.5041	3.0375	4.7621	2.2752	3.7619	5.5838	1.7552	3.3672	5.3457
	MAE	0.1138	0.2387	0.3335	0.1081	0.1902	0.2638	0.1067	0.2225	0.3333	0.1049	0.2215	0.2961
Site 2	MSE	0.0154	0.0581	0.1329	0.0139	0.0432	0.0831	0.0636	0.0892	0.1526	0.0131	0.0586	0.1311
	MAPE(%)	1.7698	3.6455	5.1838	1.6799	2.9566	4.1009	1.7593	3.5575	5.5822	1.6307	3.4444	5.2921
	MAE	0.1161	0.2403	0.3621	0.1072	0.2197	0.2901	0.1272	0.2446	0.3746	0.1207	0.2438	0.3274
Site 3	MSE	0.0161	0.0687	0.1559	0.0137	0.0575	0.1001	0.0193	0.0713	0.1671	0.0174	0.0708	0.1325
	MAPE(%)	1.6391	3.3909	5.1124	1.5125	3.1007	4.0939	1.7951	3.4511	5.2852	1.7036	3.4409	4.7401
	MAE	0.1273	0.2421	0.3844	0.1221	0.2364	0.3149	0.1385	0.2576	0.3933	0.1304	0.2447	0.3112
Site 4	MSE	0.0184	0.0667	0.1683	0.0169	0.0636	0.1128	0.0218	0.0756	0.1761	0.0193	0.0684	0.1303
	MAPE(%)	1.7106	3.2516	5.1642	1.6411	3.1774	4.2304	1.8609	3.4617	5.2849	1.7519	3.2871	4.9806

Table 9

Improvement percentages between four proposed hybrid models and SSA-BA-RBFNN, SSA-BA-GRNN, FEEMD-BA-RBFNN and FEEMD-BA-GRNN

		SSA-CG-BA-RBFNN *vs.* SSA-BA-RBFNN			SSA-CG-BA-GRNN *vs.* SSA-BA-GRNN			FEEMD-CG-BA-RBFNN *vs.* FEEMD-BA-RBFNN			FEEMD-CG-BA-GRNN *vs.* FEEMD-BA-GRNN		
		1-step	**2-step**	**3-step**	**1-step**	**2-step**	**3-step**	**1-step**	**2-step**	**3-step**	**1-step**	**2-step**	**3-step**
Site 1	ξ_{MAE}(%)	-6.694	-3.881	-3.015	-15.394	-2.643	-17.759	-35.688	-18.668	-15.294	-21.517	-10.021	-41.113
	ξ_{MSE}(%)	-12.534	-7.833	-5.940	-28.947	-5.825	-16.896	-11.594	-15.618	-5.513	-38.834	-19.261	-1.0928
	ξ_{MAPE}(%)	-6.686	-3.941	-3.101	-15.431	-2.788	-10.739	-16.257	-9.543	-3.376	-21.649	-10.131	-12.037
Site 2	ξ_{MAE}(%)	-11.159	-9.719	-6.417	-28.492	-7.098	-5.876	-11.153	-9.034	-1.380	-17.826	-15.079	-3.3772
	ξ_{MSE}(%)	-20.779	-4.475	-12.491	-48.921	-13.657	-11.191	-83.176	-45.179	-10.616	-32.061	-27.986	-25.476
	ξ_{MAPE}(%)	-11.081	-8.150	-6.428	-28.472	-7.018	-5.933	-16.228	-11.503	-5.872	-17.796	-15.143	-15.838
Site 3	ξ_{MAE}(%)	-19.207	-8.656	-10.494	-20.615	-20.118	-10.823	-24.921	-13.041	-7.315	-25.186	-14.356	-4.6731
	ξ_{MSE}(%)	-34.782	-16.448	-19.692	-37.226	-36.173	-20.579	-44.041	-24.544	-14.123	-44.253	-26.694	-12.528
	ξ_{MAPE}(%)	-19.169	-8.656	-10.541	-20.456	-20.182	-10.733	-24.917	-12.969	-7.319	-25.182	-14.333	-7.0716
Site 4	ξ_{MAE}(%)	-21.366	-9.418	-5.489	-24.733	-14.086	-9.622	-24.763	-12.616	-7.323	-25.231	-9.481	-6.7159
	ξ_{MSE}(%)	-38.043	-17.841	-10.754	-43.195	-26.258	-18.262	-43.578	-23.677	-14.082	-44.041	-18.274	-26.401
	ξ_{MAPE}(%)	-21.384	-9.365	-5.441	-24.763	-14.197	-9.574	-24.724	-12.641	-7.353	-25.229	-9.455	-13.659

Tables 10-13 ~~indicates~~ indicate the following:

(a) GRNN and ARIMA are the most and least accurate forecasting models, respectively, among RBFNN, GRNN and ARIMA in one-step to three-step prediction of the data from four sites.

(b) The four proposed models are more accurate than ELM and SVM. ELM is more accurate than RBFNN, GRNN, ARIMA and SVM.

(c) Based on the one-step to three-step prediction of RBFNN, from four sites, SSA-CG-BA-RBFNN decreases 105.591%, 65.3882% and 42.2669%; 120.131%, 57.6424% and 50.8865%; 158.419%, 77.7006% and 49.7562%; 156.722%, 85.9658% and 41.8967% MAPE values, respectively. And FEEMD-CG-BA-RBFNN decreases 166.848%, 81.9731% and 70.6989%; 188.299%, 92.0083% and 89.7268%; 184.582%, 122.397% and 87.4155%; 179.614%, 101.027% and 81.1342% MAPE values, respectively.

(d) In the one-step to three-step prediction, the MAPE promoted percentages from four sites of SSA-CG-BA-GRNN and FEEMD-CG-BA-GRNN by GRNN are -78.1504%, -57.9035% and -34.4856% and -146.822%, -77.5652% and -54.3086%; -135.052%, -67.6619% and -39.2909% and -158.426%, -80.5974% and -64.3257%; -154.029%, -83.2562% and -39.8232% and -168.618%, -86.7252% and -55.4882%; -146.459%, -81.2308% and -41.5171% and -163.562%, -84.1414% and -61.13065%, respectively.

(e) For Site 1, the MAPE promoted percentages, in the one-step to three-step prediction, from four sites of ARIMA with SSA-CG-BA-RBFNN, FEEMD-CG-BA-RBFNN, SSA-CG-BA-GRNN and FEEMD-CG-BA-GRNN are -1221.677%, -147.985% and -117.011%; -317.523%, -172.853% and -160.381%; -178.743%, -136.762% and -105.141%; -286.191%, -166.243% and -135.379%, respectively.

(f) For Site 2, the MAPE promoted percentages, in the one-step to three-step prediction, from four sites of ARIMA with SSA-CG-BA-RBFNN, FEEMD-CG-BA-RBFNN, SSA-CG-BA-GRNN and FEEMD-CG-BA-GRNN are -238.940%, -143.343% and -127.044%; -343.899%, -196.392% and -185.488%; -261.914%, -158.809% and -109.595% and -297.903%, -178.777% and -147.266%, respectively.

(g) The MAPE promoted percentages, for Site 3 in the one-step to three-step prediction, from four sites of ARIMA with SSA-CG-BA-RBFNN, FEEMD-CG-BA-RBFNN, SSA-CG-BA-GRNN and FEEMD-CG-BA-GRNN are -323.933%, -162.826% and -140.647%; -366.852%, -228.935% and -201.163%; -316.731%, -171.043% and -124.685% and -340.663%, -176.174% and -149.858%, respectively.

(h) In the one-step to three-step prediction for Site 4, the MAPE promoted percentages from four sites of ARIMA with SSA-CG-BA-RBFNN, FEEMD-CG-BA-RBFNN, SSA-CG-BA-GRNN and FEEMD-CG-BA-GRNN are -304.528%, -167.038% and -130.607%; -340.601%, -188.666% and -194.374%; -288.357%, -160.239% and -129.992%; -315.306%, -164.418% and -161.865%, respectively.

Remark

By comparing SSA-CG-BA-RBFNN, SSA-CG-BA-GRNN, FEEMD-CG-BA-RBFNN and FEEMD-CG-BA-GRNN with ELM, SVM, RBFNN, GRNN and ARIMA, the forecasting performance of the proposed four hybrid models are better than that of the single models.

Table 10

Forecasting performance of RBFNN, GRNN and ARIMA

		RBFNN			**GRNN**			**ARIMA**		
		1-step	**2-step**	**3-step**	**1-step**	**2-step**	**3-step**	**1-step**	**2-step**	**3-step**
	MAE	0.2523	0.3171	0.4377	0.1861	0.2947	0.3979	0.2912	0.4418	0.6071
Site 1	MSE	0.0707	0.1117	0.2131	0.0385	0.0966	0.1761	0.0943	0.2169	0.4095
	MAPE(%)	4.6003	5.7811	7.9794	3.3943	5.3733	7.2559	5.3109	8.0568	11.068
	MAE	0.2938	0.3846	0.5073	0.2229	0.3395	0.4707	0.3431	0.5241	0.7085
Site 2	MSE	0.1031	0.1767	0.3073	0.0594	0.1377	0.2646	0.1405	0.3279	0.5996
	MAPE(%)	4.5687	5.9792	7.8871	3.4642	5.2785	7.3189	5.3339	8.1481	11.013
	MAE	0.3245	0.4228	0.5418	0.2424	0.3901	0.4853	0.3981	0.5769	0.7797
Site 3	MSE	0.1253	0.2128	0.3494	0.0699	0.1811	0.2804	0.1886	0.3961	0.7233
	MAPE(%)	4.5794	5.9651	7.6461	3.4238	5.5041	6.8491	5.6167	8.1408	11.006
	MAE	0.3223	0.4522	0.5823	0.2571	0.4079	0.5157	0.4049	0.5858	0.8383
Site 4	MSE	0.1183	0.2328	0.3861	0.0753	0.1894	0.3028	0.1867	0.3906	0.8006
	MAPE(%)	4.3311	6.0751	7.8223	3.4524	5.4806	6.9291	5.4401	7.8699	11.261

Table 11

Forecasting performance of ELM and SVM

		ELM			SVM		
		1-step	**2-step**	**3-step**	**1-step**	**2-step**	**3-step**
	MAE	0.1774	0.2756	0.4566	0.2614	0.3015	0.4118
Site 1	MSE	0.0381	0.0905	0.1645	0.0495	0.1166	0.1849
	MAPE(%)	3.1044	5.0019	6.9985	3.6498	5.7654	7.6811
	MAE	0.1956	0.3141	0.4415	0.2415	0.3124	0.4845
Site 2	MSE	0.0428	0.1124	0.2561	0.0469	0.1244	0.3146
	MAPE(%)	3.2107	5.0163	6.9875	3.7105	5.8647	7.6447
	MAE	0.2014	0.3421	0.4685	0.2768	0.3216	0.4975
Site 3	MSE	0.0419	0.1031	0.2541	0.0684	0.1467	0.3017
	MAPE(%)	3.1964	5.1651	6.9541	3.8004	5.9451	7.1847
	MAE	0.2051	0.3518	0.5251	0.2617	0.5131	0.5347
Site 4	MSE	0.0423	0.1179	0.2741	0.0751	0.2015	0.3241
	MAPE(%)	3.1553	5.1618	6.9144	3.8117	5.9614	7.1874

Table 12

Improvement percentages between four proposed hybrid models and RBFNN and GRNN

		SSA-CG-BA-RBFNN *vs.* RBFNN			FEEMD-CG-BA- RBFNN *vs.* RBFNN			SSA-CG-BA-GRNN *vs.* GRNN			FEEMD-CG-BA-GRNN *vs.* GRNN		
		1-step	**2-step**	**3-step**	**1-step**	**2-step**	**3-step**	**1-step**	**2-step**	**3-step**	**1-step**	**2-step**	**3-step**
	ξ_{MAE}(%)	-105.408	-65.2832	-42.1579	-166.619	-81.8014	-70.4799	-77.7459	-57.6779	-34.2896	-146.491	-77.4232	-54.1651
Site 1	ξ_{MSE}(%)	-323.076	-173.654	-102.181	-612.963	-231.959	-191.074	-215.573	-148.329	-80.2457	-511.111	-215.686	-137.973
	ξ_{MAPE}(%)	-105.591	-65.3882	-42.2669	-166.848	-81.9731	-70.6989	-78.1504	-57.9035	-34.4856	-146.822	-77.5652	-54.3086
	ξ_{MAE}(%)	-120.474	-57.541	-50.817	-188.357	-92.134	-89.569	-135.127	-67.737	-39.302	-158.585	-80.489	-64.523
Site 2	ξ_{MSE}(%)	-386.885	-148.108	-127.515	-736.619	-269.169	-258.537	-455.141	-181.595	-93.988	-567.416	-226.303	-170.829
	ξ_{MAPE}(%)	-120.131	-57.642	-50.887	-188.299	-92.008	-89.727	-135.052	-67.662	-39.291	-158.426	-80.597	-64.326
	ξ_{MAE}(%)	-158.422	-77.722	-49.738	-184.841	-122.279	-87.592	-153.822	-83.404	-39.775	-168.439	-86.830	-55.495
Site 3	ξ_{MSE}(%)	-565.714	-215.505	-123.961	-712.791	-393.461	-252.704	-547.222	-236.617	-95.401	-620.619	-248.941	-141.933
	ξ_{MAPE}(%)	-158.419	-77.701	-49.756	-184.582	-122.397	-87.416	-154.029	-83.256	-39.823	-168.618	-86.725	-55.488
	ξ_{MAE}(%)	-156.843	-86.001	-41.949	-179.761	-100.837	-81.202	-146.737	-81.208	-41.482	-163.692	-84.154	-77.644
Site 4	ξ_{MSE}(%)	-560.526	-245.621	-101.597	-684.375	-303.838	-228.416	-512.195	-228.249	-100.132	-597.222	-238.819	-215.746
	ξ_{MAPE}(%)	-156.722	-85.966	-41.897	-179.614	-101.027	-81.134	-146.459	-81.231	-41.517	-163.562	-84.141	-61.131

Table 13

Improvement percentages between four proposed hybrid models and ARIMA

		SSA-CG-BA-RBFNN *vs.* ARIMA			FEEMD-CG-BA- RBFNN *vs.* ARIMA			SSA-CG-BA-GRNN *vs.* ARIMA			FEEMD-CG-BA-GRNN *vs.* ARIMA		
		1-step	**2-step**	**3-step**	**1-step**	**2-step**	**3-step**	**1-step**	**2-step**	**3-step**	**1-step**	**2-step**	**3-step**
	ξ_{MAE}(%)	221.412	147.784	116.899	317.192	172.548	160.111	178.128	136.383	104.893	285.695	165.984	135.218
Site 1	ξ_{MSE}(%)	936.263	514.447	370.149	1646.29	645.361	576.859	672.951	457.583	319.142	1396.82	608.823	453.378
	ξ_{MAPE}(%)	221.677	147.985	117.011	317.523	172.853	160.381	178.743	136.762	105.141	286.191	166.243	135.379
	ξ_{MAE}(%)	239.367	143.201	127.011	343.855	196.604	185.341	261.919	158.942	109.677	298.027	178.628	147.641
Site 2	ξ_{MSE}(%)	1051.63	490.810	415.563	1878.87	779.089	712.466	1213.08	570.552	339.589	1478.65	677.014	513.715
	ξ_{MAPE}(%)	238.940	143.343	127.044	343.899	196.392	185.488	261.914	158.809	109.595	297.903	178.777	147.266
	ξ_{MAE}(%)	324.413	162.824	140.573	367.803	228.718	201.392	316.858	171.227	124.568	340.863	176.293	149.823
Site 3	ξ_{MSE}(%)	1696.19	590.069	477.715	2093.02	979.292	809.811	1646.29	636.245	404.041	1844.33	663.198	524.072
	ξ_{MAPE}(%)	323.933	162.826	140.647	366.852	228.935	201.163	316.731	171.043	124.685	340.663	176.174	149.858
	ξ_{MAE}(%)	304.495	167.122	130.746	340.588	188.429	194.554	288.579	160.239	129.986	315.282	164.469	188.771
Site 4	ξ_{MSE}(%)	1537.71	612.773	433.023	1844.79	732.836	768.329	1417.88	576.949	429.147	1628.71	598.747	734.827
	ξ_{MAPE}(%)	304.528	167.038	130.607	340.601	188.666	194.374	288.357	160.239	129.992	315.306	164.418	161.865

6.4 Experiment III: Persistence prediction test

To evaluate the proposed model, in this part a persistence prediction test is employed. In this test, the proposed model is used to output 100 continuous data. The forecasting results presented in **Table 14** show that SSA-CG-BA-GRNN could always keep an ~~accurate~~ high forecasting performance in this test.

Table 14

Forecasting results of the persistence prediction test

No.	Actual value (m/s)	Forecasting value (m/s)	MAPE (%)	No.	Actual value (m/s)	Forecasting value (m/s)	MAPE (%)
1	3.8	3.8418	1.0988	51	4.5	4.4465	1.1881
2	3.8	3.7554	1.1742	52	4.8	4.7456	1.1330
3	3.8	3.7536	1.2200	53	4.6	4.6508	1.1038
4	3.9	3.8576	1.0867	54	4.1	4.0504	1.2091
5	4.1	4.1469	1.1439	55	4.3	4.3519	1.2079
6	3.7	3.6552	1.2109	56	4.4	4.3468	1.2095
7	3.1	3.1386	1.2440	57	4.3	4.2474	1.2242
8	3.2	3.1592	1.2737	58	4.2	4.1463	1.2787
9	2.2	2.1748	1.1450	59	4.4	4.4485	1.1012
10	2.1	2.1252	1.2022	60	4.3	4.3470	1.0927
11	2.2	2.1744	1.1647	61	5.2	5.2608	1.1697
12	2	2.0227	1.1333	62	6.2	6.2764	1.2327
13	2.5	2.5284	1.1362	63	6.4	6.3210	1.2344
14	2.4	2.4285	1.1854	64	6.2	6.1210	1.2745
15	2.3	2.3289	1.2551	65	5.4	5.4598	1.1078
16	2.8	2.7645	1.2687	66	4.2	4.1539	1.0988
17	3.5	3.4555	1.2715	67	4.1	4.0514	1.1861
18	4	4.0486	1.2152	68	4.4	4.3482	1.1770
19	4.2	4.2510	1.2144	69	5.4	5.4656	1.2143
20	3.8	3.7584	1.0936	70	5.9	5.8301	1.1840
21	2.8	2.8315	1.1248	71	6	6.0666	1.1100
22	2.8	2.7650	1.2489	72	6	5.9321	1.1324
23	3.1	3.1383	1.2361	73	6.4	6.4788	1.2310
24	3.1	3.0665	1.0813	74	5.9	5.9689	1.1685
25	3.6	3.5583	1.1574	75	6.3	6.2274	1.1518
26	5.6	5.5395	1.0802	76	6.1	6.0293	1.1589
27	5	5.0582	1.1649	77	6	5.9268	1.2208
28	4.8	4.8592	1.2340	78	6.1	6.1661	1.0839
29	4.6	4.6569	1.2369	79	6.3	6.3734	1.1649
30	3.4	3.4370	1.0872	80	6.4	6.4716	1.1194
31	4.3	4.3526	1.2244	81	6.8	6.7207	1.1660
32	4.6	4.6511	1.1105	82	7.1	7.0178	1.1582
33	4.3	4.3517	1.2015	83	7.1	7.0177	1.1594
34	4.4	4.4540	1.2277	84	6.9	6.8151	1.2310

35	4.3	4.3543	1.2635	85	6.2	6.2696	1.1232
36	3.4	3.4419	1.2331	86	5.7	5.6276	1.2699
37	2.4	2.4273	1.1375	87	5.7	5.7692	1.2143
38	2.3	2.3275	1.1952	88	5.6	5.6698	1.2467
39	2.6	2.5691	1.1893	89	5.7	5.6365	1.1135
40	2.8	2.8338	1.2089	90	5.8	5.7259	1.2780
41	2.6	2.5684	1.2158	91	5.6	5.5296	1.2569
42	2.7	2.6657	1.2690	92	5.9	5.8345	1.1110
43	2.8	2.8342	1.2219	93	5.8	5.8674	1.1614
44	3.6	3.6397	1.1039	94	5.6	5.5303	1.2451
45	4.1	4.0520	1.1700	95	5.3	5.2394	1.1437
46	4.6	4.6558	1.2124	96	5.2	5.1429	1.0980
47	4.4	4.3494	1.1500	97	5.3	5.3587	1.1073
48	3.9	3.8546	1.1632	98	5.4	5.3363	1.1790
49	4.1	4.0489	1.2466	99	5.4	5.4637	1.1790
50	3.7	3.7445	1.2027	100	4.8	4.8524	1.0910

6.5 Experiment IV: Diebold-Mariano (DM)-test and forecasting validity degree (FVD)

The ~~Diebold-Mariano (DM)~~ DM test and FVD are conducted to further evaluate the levels of accuracy achieved by the proposed hybrid models (as shown in **Fig. 7**).

DM test which is a comparison test focusing on predictive accuracy, could be used to compare the forecasting performance of the proposed hybrid model with others. For more details, one can refer [55], which provides a complete description of the DM test theory.

FVD can be measured not only by the square sum of forecasting error but also by the mean and mean squared deviation of the forecasting accuracy. It is a useful tool to evaluate the forecasting accuracy of the model. For more details, one can refer [56], which provides a complete description of the DM test theory.

The results given in **Table 15** indicate the following:

(a) SSA-CG-BA-RBFNN is more accurate than RBFNN and ARIMA at the 10% significance level, more accurate than SSA-BA-RBFNN, FEEMD-BA-RBFNN, SSA-BA-GRNN, FEEMD-BA-GRNN and GRNN at the 5% significance level, and more accurate than FEEMD-CG-BA-RBFNN at the 1% significance level.

(b) FEEMD-CG-BA-RBFNN is more accurate than RBFNN, GRNN and ARIMA at the 10% significance level and more accurate than SSA-BA-RBFNN, FEEMD-BA-RBFNN, SSA-BA-GRNN and FEEMD-BA-GRNN at the 5% significance level.

(c) SSA-CG-BA-GRNN is the most accurate model among these models. It is more accurate than SSA-CG-BA-RBFNN, FEEMD-CG-BA-RBFNN and FEEMD-CG-BA-GRNN at the 1% significance level, more accurate than SSA-BA-RBFNN, FEEMD-BA-RBFNN, SSA-BA-GRNN and FEEMD-CG-BA-GRNN at the 5% significance level, and more accurate than

RBFNN, GRNN and ARIMA at the 10% significance level.

(d) FEEMD-CG-BA-GRNN is more accurate than SSA-CG-BA-RBFNN and FEEMD-CG-BA-RBFNN at the 1% significance level, more accurate than SSA-BA-RBFNN, FEEMD-BA-RBFNN, SSA-BA-GRNN and FEEMD-CG-BA-GRNN at the 5% significance level, and more accurate than RBFNN, GRNN and ARIMA at the 10% significance level.

Table 15

Results for the DM test

		SSA-CG-BA-RBFNN
	FEEMD-CG-BA-RBFNN	1.773275*
	SSA-CG-BA-GRNN	1.298743
	FEEMD-CG-BA-GRNN	1.480342
	SSA-BA-RBFNN	2.092264**
	FEEMD-BA-RBFNN	2.043212**
	SSA-BA-GRNN	1.999822**
	FEEMD-BA-GRNN	1.970851**
	RBFNN	3.673214***
	GRNN	2.570125**
	ARIMA	5.662563***
		FEEMD-CG-BA-RBFNN
	SSA-CG-BA-RBFNN	1.577545
	SSA-CG-BA-GRNN	1.290934
	FEEMD-CG-BA-GRNN	1.400953
	SSA-BA-RBFNN	1.992563**
DM-test	FEEMD-BA-RBFNN	2.001252**
	SSA-BA-GRNN	1.900823**
	FEEMD-BA-GRNN	1.980123**
	RBFNN	3.356216***
	GRNN	2.790325***
	ARIMA	5.467216***
		SSA-CG-BA-GRNN
	SSA-CG-BA-RBFNN	1.933213*
	FEEMD-CG-BA-RBFNN	1.956331*
	FEEMD-CG-BA-GRNN	1.763224*
	SSA-BA-RBFNN	2.456424**
	FEEMD-BA-RBFNN	2.473563**
	SSA-BA-GRNN	2.345621**
	FEEMD-BA-GRNN	2.578142**
	RBFNN	3.809438***
	GRNN	3.155621***
	ARIMA	5.779335***

	FEEMD-CG-BA-GRNN
SSA-CG-BA-RBFNN	1.893781*
FEEMD-CG-BA-RBFNN	1.960031*
SSA-CG-BA-GRNN	1.602371
SSA-BA-RBFNN	2.244341**
FEEMD-BA-RBFNN	2.389023**
SSA-BA-GRNN	2.109824**
FEEMD-BA-GRNN	2.100231**
RBFNN	3.673214***
GRNN	2.700915***
ARIMA	5.662563***

* indicates the 1% significance level; ** indicates the 5% significance level; *** indicates the 10% significance level.

FVD is measured to evaluate the forecasting accuracy of the hybrid models and the other six comparison models. A more accurate forecasting model leads to a larger FVD value. The results presented in **Table 16** show that the FVD value for the SSA-CG-BA-GRNN model is larger than those of the comparison models.

Table 16
Results for FVD

Model	**FVD**		
	1-step	**2-step**	**3-step**
SSA-CG-BA-RBFNN	98.5264	96.8396	95.1481
FEEMD-CG-BA-RBFNN	98.4681	96.8553	94.8889
SSA-CG-BA-GRNN	**98.7722**	**97.2742**	**96.1030**
FEEMD-CG-BA-GRNN	98.6750	97.0318	95.5347
SSA-BA-RBFNN	98.2778	96.5825	94.8191
FEEMD-BA-RBFNN	98.0774	96.4420	94.5660
SSA-BA-GRNN	98.4156	96.9320	95.7032
FEEMD-BA-GRNN	98.2897	96.6151	94.9104
RBFNN	95.4801	94.0499	92.1663
GRNN	96.5663	94.5909	92.9118
ARIMA	94.5746	91.9461	88.9130

Table 17
Total computation time of each ~~models~~ model

Model	**CPU time (s)**
SSA-CG-BA-RBFNN	38.6145
FEEMD-CG-BA-RBFNN	39.1547
FEEMD-CG-BA-GRNN	31.0245
SSA-CG-BA-GRNN	28.6414
SSA-BA-RBFNN	23.6554

FEEMD-BA-RBFNN	24.0046
SSA-BA-GRNN	22.0894
FEEMD-BA-GRNN	23.1663
RBFNN	16.2461
GRNN	14.2541
ARIMA	8.9564
ELM	12.6791
SVM	18.4989

Remark

Based on the results from the above two methods, the forecasting performance of SSA-CG-BA-GRNN has been globally evaluated. From the results of the DM test and FVD, one can see that SSA-CG-BA-GRNN is the most accurate forecasting model among the proposed forecasting architecture for multi-step wind speed forecasting. As shown in **Table 17**, SSA-CG-BA-GRNN is ~~faster~~ more efficient than FEEMD-CG-BA-GRNN, SSA-CG-BA-RBFNN and FEEMD-CG-BA-RBFNN. The relation between the wind speed and wind power generation could be expressed as the following equation:

$$P_a = \left\{ \frac{\exp\left[-\left(v_c/c\right)^k\right] - \exp\left[-\left(v_r/c\right)^k\right]}{\left(v_r/c\right)^k - \left(v_c/c\right)^k} - \exp\left[-\left(v_f/c\right)^k\right] \right\} \times P_r \tag{2}$$

where P_a is the average power output of the wind turbine (kW), P_r is the rated electrical power of the wind turbine (kW), v_c is the cut-in wind speed (m/s), v_f is the cut-off wind speed (m/s), v_r is the nominal wind speed (m/s), and c is the Weibull scale parameter (m/s). It is observed that the accurate wind speed forecasting plays an important role in the wind power generation.

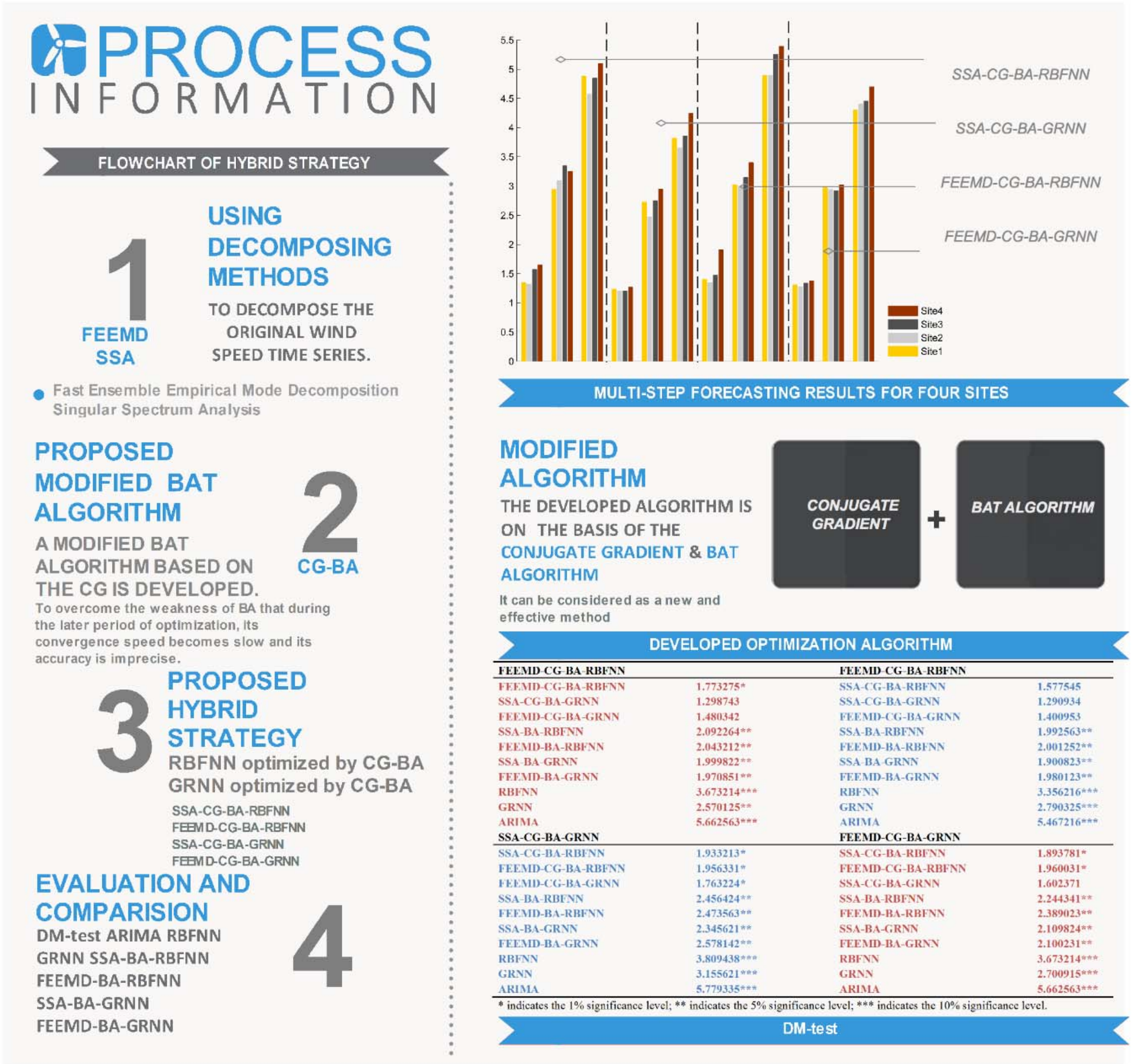

Fig. 7. Process of hybrid forecasting strategy and DM test results.

7. Conclusion

As one of the most promising potential renewable energies, wind energy has been a focus of many scientists and researchers and supported by almost every government across the world. To integrate wind energy into the power system, it is important to forecast wind power generation. Wind speed is affected by various environmental factors, so wind speed data present high fluctuations, autocorrelation and stochastic volatility, and it is difficult to forecast wind speed using a single model. In this paper, four hybrid models based on two decomposition algorithms, SSA and FEEMD, and two neural networks, RBFNN and GRNN, are proposed for multi-step wind speed forecasting. Meanwhile, to improve the performance of the neural networks, a new improved BA algorithm, CG-BA, based on CG is proposed to optimize the initial weights and thresholds of neural networks. Based on a series of forecasting results, the DM test and FVD, the following can be concluded: (a) the hybrid SSA-CG-BA-GRNN model is the most accurate model among the four proposed models in multi-step wind speed forecasting; (b) the decomposition algorithm SSA is better than FEEMD in this study; (c) the performance of the single model GRNN is more accurate than RBFNN and ARIMA.

Thus, the proposed SSA-CG-BA-GRNN model, which has the highest precision, is a promising model for use in the future. This hybrid model can also be applied in many other fields, such as tourism demand forecasting, product sales forecasting, power load forecasting, and traffic flow forecasting.

Acknowledgements

This work was supported by the National Natural Science Foundation of China (Grant No. 61331007 and 61471105) and 973 Project (No. 613273).

Appendix A

Appendix A1 SSA and FEEMD

SSA is a novel nonparametric method, which is employed in the analysis of time series and combines multivariate statistic and probability theory, and it is often used for identifying and extracting periodic, quasi-periodic and oscillatory components from the primal data [28]. Standard SSA performs four steps, which include embedding, singular value decomposition, grouping and diagonal averaging. However, the first two steps are also called the time series decomposition, and steps three and four are known as the reconstruction. For more details, one can refer [28, 44], which provides a complete description of the SSA theory.

FEEMD is an extension of the empirical mode decomposition [45] and ensemble empirical mode decomposition techniques [46]. The fast ensemble empirical mode decomposition technique is a time-domain decomposing method, which can convert a group of time series into multiple empirical modes, named as the intrinsic mode functions (IMFs). $y(t)$ is the time series, it can be decomposed and expressed using the following formula:

$$y(t) = \sum_{j=1}^{n} \mathbf{IMF}_j(t) + r_n(t) \tag{A1}$$

where $\mathbf{IMF}_j(t)$, j=1, 2, …, n, is the intrinsic mode function (i.e., local oscillation) based on empirical mode decomposition and $r_n(t)$ is the nth residue (i.e., local trend). For more details, one can refer [47], which provides a complete description of the SSA theory.

Appendix B

Appendix B1 Standard RBFNN

Definition 1. Cluster centers were composed of elements $m_i^j\left(j=1-n\right)$ from the center vector m_i, which is in the input space.

Definition 2. With elements I_j (j = 1-n), the distance measure is used to determine how far the center vector m^i is from an input vector I. The popular distance measure is the Euclidian distance, defined as

$$d_i = \sqrt{\sum_{j=1}^{n} k_j^i \left(I_j - m_j^i\right)^2} \tag{B1}$$

where k_j^i is the (i, j)th element of the shape matrix K, defined as the inverse of the covariance matrix:

$$k_j^i = \frac{h_j^i}{\left(\sigma_j^i\right)^2} \tag{B2}$$

where h_j^i is the correlation coefficient, and σ_j^i represents the marginal standard deviation.

Definition 3. A transfer function transforms the Euclidian summation d_j (i = 1-m) and gives an output for each node. The output generated by the hidden layer was from the input layer via a distance measure of Eq. (3) and a transfer function. A weighted sum of the outputs of $\phi(d_i)$ from the hidden layer processed the output of the network, i.e.,

$$O = w_0 + \sum_{i=1}^{m} w_i \phi(d_i) \tag{B3}$$

Appendix B2 Standard GRNN

Definition 1. The input layer accepts information and also stores an input vector X, whose dimension m equals the number of input layer neurons. The pattern layer is then fed the data that comes from the input neurons of the input layer. A nonlinear transformation, which transforms the input space into the pattern space, was used by the pattern layer. The neurons of the pattern layer can remember the relation between the input neuron and the proper response of the pattern layer, in which the number of neurons is equal to the number of training samples n. The pattern Gaussian function of p_i is expressed as

$$p_i = \exp\left[-\frac{(X - X_i)^T (X - X_i)}{2\sigma^2}\right] (i = 1, 2, \ldots, n) \tag{B4}$$

where σ represents the spread parameter, and X is the network's input variable. In the pattern layer, X_i is a specific training sample of neuron i.

Definition 2. S_s and S_w are the two summations of the summation layer. The simple summation S_s is used to calculate the arithmetic sum from the outputs that belong to the pattern layer, and i is the interconnection weight of the simple summation. The weighted summation S_w is used to calculate the weighted sum from the outputs that belong to the pattern layer, and w is the interconnection weight of the weighted summation. The transfer functions can be described by Eq. (6) and (7):

$$S_s = \sum_{t=1} p_t, \qquad t = 1 \ldots n \tag{B5}$$

$$S_{wt} = \sum_{t=1} w_t p_t, \qquad t = 1 \ldots n \tag{B6}$$

where w_t is the weight of pattern neuron t that is connected to the summation layer. **Definition 3.** In the output layer, the number of neurons is equal to the dimension k of the output vector Y. In the summation layer, after the summations, the output absorbs the neurons, and the output Y of the output neurons can be computed as

$$\hat{Y}_o = S_s / S_{wo}, \qquad o = 1 \ldots k \tag{B7}$$

If the training set is given, the spread parameter R is the only parameter that must be confirmed.

Appendix C

Appendix C1 Accuracy estimating indexes

The detailed equations of MAE MSE and MAPE are given in **Table C1**.

Table C1

Three metric rules

Metric	Definition	Equation
MAE	The average absolute forecast error of n times forecast results	$\mathbf{MAE} = \frac{1}{N}\sum_{n=1}^{N}\left\|y_n - \hat{y}_n\right\|$
MSE	The average of the prediction error squares	$\mathbf{MSE} = \frac{1}{N}\sum_{n=1}^{N}\left(y_n - \hat{y}_n\right)^2$
MAPE	The average of absolute error	$\mathbf{MAPE} = \frac{1}{N}\sum_{n=1}^{N}\left\|\frac{y_n - \hat{y}_n}{y_n}\right\| \times 100\%$

where y_n and $\hat{y}_n$ denote the actual value and predicted value, respectively, of the nth data for the performance estimate, and N is the length of the dataset to compare and evaluate.

Additionally, to obtain the detailed promoting percentages when comparing two forecasting, i.e. model 1 and model 2, three percentage error indexes are also defined as follows:

$$\xi_{MAE} = \frac{MAE_2 - MAE_1}{MAE_1} \times 100\% \quad \text{(C1)}$$

$$\xi_{MSE} = \frac{MSE_2 - MSE_1}{MSE_1} \times 100\% \quad \text{(C2)}$$

$$\xi_{MAPE} = \frac{MAPE_2 - MAPE_1}{MAPE_1} \times 100\% \quad \text{(C3)}$$

The negative value of ξ_{MAE}(%) means model 2 decreases $|\xi_{MAE}|$% MAE value based on model 1, the positive value of ξ_{MAE}(%) means model 2 increases $|\xi_{MAE}|$% MAE value based on model 1. So do ξ_{MSE}(%) and ξ_{MAPE}(%).

References:

[1] Yesilbudak M, Sagiroglu S, Colak I. A new approach to very short term wind speed prediction using k -nearest neighbor classification. Energy Conversion & Management, 2013, 69(69):77-86.

[2] Meng, A., Ge, J., Yin, H., Chen, S. Wind speed forecasting based on wavelet packet decomposition and artificial neural networks trained by crisscross optimization algorithm. Energy Conversion & Management, 2016, 114:75-88.

[3] Ozay C, Celiktas M S. Statistical analysis of wind speed using two-parameter Weibull distribution in Alaçatı region. Energy Conversion & Management, 2016, 121:49-54.

[4] Liu, H., Tian, H. Q., Li, Y. F., Zhang, L. Comparison of four Adaboost algorithm based artificial neural networks in wind speed predictions. Energy Conversion & Management, 2015, 92(92):67-81.

[5] Zhao ZY, Hu J, Zuo J. Performance of wind power industry development in China: a DiamondModel study. Renew Energy 2009;34(12):2883-91.

[6] Zhang, C., Wei, H., Zhao, X., Liu, T., Zhang, K. A Gaussian process regression based hybrid approach for short-term wind speed prediction. Energy Conversion & Management, 2016, 126:1084–1092.

[7] Liu, H., Tian H., Li Y. Four wind speed multi-step forecasting models using extreme learning machines and signal decomposing algorithms. Energy Conversion & Management, 2015, 100:16-22.

[8] Zhou J, Jing S, Gong L. Fine tuning support vector machines for short-term wind speed forecasting. Energy Conversion & Management, 2011, 52(4):1990-1998.

[9] Lei M, Shiyan L, Chuanwen J, Hongling L, Yan Z. A review on the forecasting of wind speed and generated power. Renew Sustain Energy Rev 2009;13(4):915-20.

[10] Landberg L. Short-term prediction of the power production from wind farms. J Wind Eng Ind Aerodyn 1999;80:207-20.

[11] Alexiadis MC, Dokopoulos PS, Sahsamanoglou HS, Manousaridis IM. Short term forecasting of wind speed and related electrical power. Solar Energy 1998;63(1):61-8.

[12] Negnevitsky M, Potter CW. Innovative short-term wind generation prediction techniques. In: Proceedings of the power systems conference and exposition; 2006. p. 60-5.
[13] Riahy GH, Abedi M. Short term wind speed forecasting for wind turbine applications using linear prediction method. Renew Energy 2008;33(1):35-41.
[14] Ma L, Luan SY, Jiang CW, Liu HL, Zhang Y. A review on the forecasting of wind speed and generated power. Renew Sustain Energy Rev 2009;13:915-20.
[15] Xiao L, Wang J, Yang X, Xiao L. A hybrid model based on data preprocessing for electrical power forecasting. International Journal of Electrical Power & Energy Systems, 2015, 64(64):311-327.
[16] Lydia, M., Kumar, S. S., Selvakumar, A. I., Kumar, G. E. P. Linear and non-linear autoregressive models for short-term wind speed forecasting. Energy Conversion & Management, 2016, 112:115-124.
[17] Noorollahi Y, Jokar M A, Kalhor A. Using artificial neural networks for temporal and spatial wind speed forecasting in Iran. Energy Conversion & Management, 2016, 115:17-25.
[18] Barbounis TG, Theocharis JB. A locally recurrent fuzzy neural network with application to the wind speed prediction using spatial correlation. Neurocomputing 2007;70(7/9):1525-42.
[19] Focken U, Lange M, Moonnich K, Waldl H-P, Georg Beyer H, Luig A. Short-term prediction of the aggregated power output of wind farms-astatistical analysis of the reduction of the prediction error by spatial smoothing effects. J Wind Eng Ind Aerodyn 2002;90(3):231-46.
[20] Niu, M., Sun S., Wu J., Yu L., Wang J. An innovative integrated model using the singular spectrum analysis and nonlinear multi-layer perceptron network optimized by hybrid intelligent algorithm for short-term load forecasting. Applied Mathematical Modelling, 2016, 40(5–6):4079-4093.
[21] Xiao L, Shao W, Wang C, Zhang K, Lu H. Research and application of a hybrid model based on multi-objective optimization for electrical load forecasting. Applied Energy, 2016, 180(C):213-233.
[22] Su, Z., Wang, J., Lu, H., Zhao, G. A new hybrid model optimized by an intelligent optimization algorithm for wind speed forecasting. Energy Conversion & Management, 2014, 85(9):443-452.
[23] Monfared M, Rastegar H, Kojabadi HM. A new strategy for wind speed forecasting using artificial intelligent methods. Renew Energy 2009;34:845-8.
[24] Cadenas E, Rivera W. Short term wind speed forecasting in La Venta, Oaxaca, México, using artificial neural networks. Renew Energy 2009;34(1):274-8.
[25] Xiao L, Shao W, Liang T, Wang C, A combined model based on multiple seasonal patterns and modified firefly algorithm for electrical load forecasting. Applied Energy, 2016, 167:135-153.
[26] Sfetsos A. A comparison of various forecasting techniques applied to mean hourly wind speed time series. Renew Energy 2000;21(1):23-35.
[27] Mohandes MA, Halawani TO, Rehman S, Hussain AA. Support vector machines for wind speed prediction. Renew Energy 2004;29:939-47.

[28] Chen N, Qian Z, Meng X. Multi-step wind speed forecasting based on wavelet and gaussian processes. Math Probl Eng 2013;2013.
[29] Liu H, Tian H-Q, Pan D-F, Li Y-F. Forecasting models for wind speed using wavelet, wavelet packet, time series and Artificial Neural Networks. Appl Energy 2013;107:191–208.
[30] Liu H, Chen C, Tian H-Q, Li Y-F. A hybrid model for wind speed prediction using empirical mode decomposition and artificial neural networks. Renew Energy 2012;48:545–56.
[31] Wang Y, Wang S, Zhang N. A novel wind speed forecasting method based on ensemble empirical mode decomposition and GA-BP neural network. presented at the IEEE power and energy society general meeting; 2013.
[32] Liu H, Tian H-Q, Li Y-F. Comparison of new hybrid FEEMD-MLP, FEEMD-ANFIS, Wavelet Packet-MLP and Wavelet Packet-ANFIS for wind speed predictions. Energy Convers Manage 2014;89:1–11.
[33] Liu H, Tian H-Q, Chen C, Li Y-F. An experimental investigation of two WaveletMLP hybrid frameworks for wind speed prediction using GA and PSO optimization. Int J Electr Power Energy Syst 2013;52(1):161–73.
[34] Poitras G, Cormier G. Wind speed prediction for a target station using neural networks and particle swarm optimization. Wind Eng 2011;35(3):369–80.
[35] Carro-Calvo L, Salcedo-Sanz S, Prieto L, Kirchner-Bossi N, Portilla-Figueras A, Jiménez-Fernández S. Wind speed reconstruction from synoptic pressure patterns using an evolutionary algorithm. Appl Energy 2012;89(1):347–54.
[36] Xiao L, Wang J, Hou R, Wu J. A combined model based on data pre-analysis and weight coefficients optimization for electrical load forecasting. Energy 2015; 82:524-549.
[37] Yang, X. S. (2010b). A new metaheuristic bat-inspired algorithm. In Nature inspired cooperative strategies for optimization (NICSO 2010). Studies in computational intelligence (Vol. 284, pp. 65–74). Berlin: Springer Verlag.
[38] Yang, X. S. (2013). Bat algorithm: Literature review and applications. International Journal of Bio-Inspired Computation, 5(3), 141–149.
[39] Du, Z. Y., & Liu, B. (2012). Image matching using a bat algorithm with mutation. Applied Mechanics and Materials, 203, 88–93.
[40] Mishra, S., Shaw, K., & Mishra, D. (2012). A new meta-heuristic bat inspired classification approach for microarray data. Procedia Technology, 4, 802–806.
[41] Musikapun, P., & Pongcharoen, P. (2012). Solving multi-stage multi-machine multiproduct scheduling problem using bat algorithm. Second international conference on management and artificial intelligence (IPEDR) (Vol. 35, pp. 98–102). Singapore: IACSIT Press.
[42] Niknam, T., Sharifinia, S., & Abaraghooee, R. A. (2013). A new enhanced bat-inspired algorithm for finding linear supply function equilibrium of GENCOs in the competitive electricity market. Energy Conversion and Management, 76, 1015–1028.
[43] Sambariya, D. K., & Prasad, R. (2014). Robust tuning of power system stabilizer for small signal stability enhancement using metaheuristic bat algorithm. International

Journal of Electrical Power & Energy Systems, 61, 229–238.

[44] Skittides C, Früh W G., Wind forecasting using Principal Component Analysis. Renewable Energy, September 2014, Vol.69, pp.365-374.

[45] NE Huang, HH Liu. The empirical mode decomposition and the hilbert spectrum for nonlinear and non-stationary time series analysis. Proceedings of the Royal Society A Mathematical Physical & Engineering Sciences, 454(1971), 903.

[46] Z Wu, NE. Huang. Ensemble empirical mode decomposition: a noise-assisted data analysis method. Advances in Adaptive Data Analysis, 1 (01) (2009) 1-41.

[47], YH Wang, CH Yeh, HWV Young, K Hu, MT Lo,. On the computational complexity of the empirical mode decomposition algorithm. Physica A Statistical Mechanics & Its Applications, 400(2) (2014) 159-167.

[48] Yang XS. A new metaheuristic bat-inspired algorithm. Nature Inspired Cooperative Strategies for Optimization (NICSO), Studies in Computational Intelligence. Springer, vol. 284; 2010. p. 65–74.

[49] Yang XS. Bat algorithm for multiobjective optimization. Int J Bio-Inspired Comput 2011;3(5):267–74.

[50] Shen, F.; Chao, J.; Zhao, J. Forecasting exchange rate using deep belief networks and conjugate gradient method. Neurocomputing. 2015, 167, 243-253.

[51] Guo XT, Zhu Y. Evolutionary neural networks based on genetic algorithms. Journal of Tsinghua university (science and technology), 2000; 40(10): 116–119.

[52] Specht DF, A general regression neural network, IEEE Transactions on Neural Networks 1991; 2 (6): 568–576.

[53] Polat O, Yildirim T. Hand geometry identification without feature extraction by general regression neural network. Expert Syst Appl 2008; 34: 845–9.

[54] Hecht-Nielsen SR, “Kolmogorov’s mapping neural network existence theorem”, in IEEE Joint Conf. on Neural Networks, New York, USA, 1987, vol. 3, pp. 11-14

[55] Diebold FX, Mariano R. Comparing predictive accuracy. J Bus Econ Stat 1995;13:253–63.

[56] Chen HY, Hou DP. “Research on superior combination forecasting model based on forecasting effective measure,” Journal of University of Science and Technology of China 2 (2002) 006.